Article

Dark Sector Flavor Symmetry: Gell-Mann–Okubo Mass Splittings for $SU(3)_{\text{dark}}$ Self-Interacting DM

Ahmed Ali [1,*]

Current Research Affiliate in Quantum Gravity and Cosmology
[1] Former Researcher, at Max-Planck-Institut für Physik, Boltzmannstraße 8, 85748 Garching bei München, DE
* Correspondence: ahmed.ali.mpi@hotmail.com

Abstract

Dark matter forms an octet under a hidden $SU(3)_{\text{dark}}$ flavor symmetry, and its mass spectrum obeys an extended Gell-Mann–Okubo formula with a *negative* hypercharge coefficient $\beta = -15\,\text{GeV}$ the same sign that the strange quark imposes in QCD. The lightest neutral member χ^0 sits at $M(\chi^0) = 165.67\,\text{GeV}$; every other state decays to it with $Q \in [0.70, 42.00]\,\text{GeV}$, completing well before big bang nucleo-synthesis. A dark Higgs triplet Δ_{dark} with $\langle\Delta_{\text{dark}}\rangle = v_\Delta = 17\,\text{GeV}$ breaks the χ^+–χ^0 degeneracy that is unavoidable in the pure GMO spectrum, generating $\Delta M(\chi^+ - \chi^0) = y_\chi v_\Delta = 1.70\,\text{GeV}$ and opening $\chi^+ \to \chi^0 + \phi^+$ with $Q = 0.70\,\text{GeV}$. Eight coupled Boltzmann equations with Griest–Seckel co-annihilation ($g_{\text{eff}} \approx 5.09$) reproduce the measured relic density $\Omega_{\text{DM}}h^2 = 0.1200 \pm 0.0012$ at $g_{\text{dark}} = 0.64 \pm 0.08$, $m_{Z'} = 17.5 \pm 2.1\,\text{GeV}$. Elastic self-scattering via t-channel exchange of the broken-$SU(3)_{\text{dark}}$ vector V_μ ($m_V = 100\,\text{GeV}$) yields $\sigma/m \propto v^{-2.1}$: $0.47 \pm 0.09\,\text{cm}^2\,\text{g}^{-1}$ at dwarf scales (resolving core-cusp and missing satellites) and $0.0044 \pm 0.0009\,\text{cm}^2\,\text{g}^{-1}$ at cluster scales (consistent with the Bullet Cluster). A partial Higgs–Stueckelberg mechanism absorbs seven of the eight would-be Goldstone bosons, giving $\Delta N_{\text{eff}} \approx 0.09$; the surviving mode drives dark acoustic oscillations at $r_{\text{DAO}} = 2.3 \pm 0.4\,\text{Mpc}$, within reach of SKA. The framework is falsifiable through twelve observables constrained by nine parameters. Two scale-independent mass ratios, $r_{21} \equiv M(\chi^{++})/M(\chi^0) = 1.089 \pm 0.005$ and $r_{31} \equiv M(\Sigma^0_{\text{dark}})/M(\chi^0) = 1.163 \pm 0.006$, are directly measurable at FCC-ee; their double ratio $r_{21}/r_{31} = 0.936$ is independent of the overall mass scale. Either a detection or a null result at any of the twelve probes listed here constitutes a definitive test of dark-sector flavor symmetry.

Keywords: CDM; Hidden $SU(3)_{\text{dark}}$; Flavor Symmetry; G-Mann–Okubo mass formula; Dark Higgs triplet; Self-interacting DM; DAO; Higgs–Stueckelberg mechanism.

Introduction

Dark matter governs structure formation on every observable scale, yet the simplest concordance assumption a collision-less, non-self-interacting relic generates systematic discrepancies at sub-galactic scales [1][2]. Core-cusp profiles in dwarf spheroidals, missing satellite counts around Milky Way analogs, and too-big-to-fail challenges collectively indicate physics beyond minimal WIMP scenarios [3][4], while null results from direct detection across four decades of mass space have placed severe constraints on canonical thermal relics [5][6].

Hadron spectroscopy provides a historical precedent. When baryon masses appeared chaotic, flavor symmetry revealed underlying order: Murray Gell-Mann and Susumu Okubo demonstrated that seemingly disparate masses obey precise relations dictated by $SU(3)$ representation theory [7][8][9]. The mass formula $M(I, Y) = a + bY + c[Y^2/4 - I(I+1)]$ not only organized known particles but predicted the Ω^- hyperon mass before its discovery [10]. A critical feature of this formula in QCD is the sign of b: because the strange quark is heavier than the up and down quarks, states with lower hypercharge (higher strangeness content) are heavier, requiring $b_{\text{QCD}} < 0$ to fit the empirical ordering nucleon $< \Sigma < \Xi$. This sign is not a convention; it encodes the dynamical hierarchy of quark masses in the flavor-symmetry-breaking sector [9][27].

If dark matter organizes into multiplets under a hidden $SU(3)_{\rm dark}$ flavor symmetry [11][12], the same algebraic machinery applies, and the same physical logic constrains the sign of the analogous dark hypercharge coefficient β. Unlike proposals invoking composite dark matter from strongly-coupled theories [13][14], the framework presented here requires no new confining gauge interactions. $SU(3)_{\rm dark}$ acts as a global symmetry spontaneously broken at scale $\Lambda_{\rm dark} \sim 200\,\text{GeV}$, generating mass hierarchies through Yukawa couplings to scalar mediators [15][16]. An auxiliary dark Higgs triplet $\Delta_{\rm dark}$, transforming in the **3** representation of the residual $SU(2)_{\rm dark}$ factor, acquires a vacuum expectation value $v_\Delta \simeq 17\,\text{GeV}$ and resolves through a Yukawa interaction the degeneracy among isospin partners that would otherwise arise at tree level in the extended GMO framework. A partial Higgs–Stueckelberg mechanism described in Appendix H absorbs seven of the eight would-be Goldstone bosons from $SU(3)_{\rm dark}$ breaking into massive dark gauge bosons, retaining one light pseudo-Goldstone ϕ_1 to mediate dark acoustic oscillations while ensuring $\Delta N_{\rm eff} \ll 0.17$.

Three qualitative consequences distinguish this scenario from both minimal WIMP models and generic self-interacting dark matter proposals. First, the lightest multiplet member χ^0 is absolutely stable by a combination of charge neutrality, kinematic stability, and a topological argument based on the second homotopy group of the vacuum manifold [11][12]; every other octet state decays within timescales shorter than $10^{-9}\,\text{s}$, well before big bang nucleosynthesis. Second, the triplet-induced mass splitting $\Delta M(\chi^+ - \chi^0) = 1.70\,\text{GeV}$ lifts the charged state χ^+ above χ^0 and opens a kinematically accessible decay channel that, absent $\Delta_{\rm dark}$, would be forbidden. Third, mass splittings ranging from 1.70 to 43.00 GeV enable velocity-dependent self-interactions with the $\sigma/m \propto v^{-2}$ profile that simultaneously resolves dwarf and cluster anomalies [18][19].

This study organized as follows: Section 2 establishes the $SU(3)_{\rm dark}$ algebra, derives the extended mass formula incorporating dark isospin, dark hypercharge, and darkicity, demonstrates why $\beta < 0$ from the QCD analogy and the intra-multiplet stability condition, presents the dark Higgs triplet sector, and solves for the complete octet eigenvalue spectrum. Section 3 solves coupled Boltzmann equations for the eight-component freeze-out system. Section 4 computes self-interaction cross-sections from t-channel vector-boson exchange. Section 5 analyses matter power spectrum modifications, halo mass functions, and dark acoustic oscillations. Section 6 enumerates twelve falsifiable predictions. Section 7 discusses comparisons with competing frameworks, open theoretical questions, and cosmological phase transition gravitational waves. Section 8 concludes. Appendices provide detailed derivations, numerical methods, and the partial Higgs–Stueckelberg construction.

1. Mathematical Formulation

The Gell-Mann–Okubo relation emerges from representation theory. Consider generators T^a ($a = 1, \ldots, 8$) of $SU(3)$ satisfying $[T^a, T^b] = if^{abc}T^c$ with structure constants f^{abc}. Casimir operators $C_2 = T^aT^a$ and $C_3 = d^{abc}T^aT^bT^c$ label irreducible representations [8]. For the adjoint (octet) representation with dimension $d = 8$, $C_2 = 3$ identically. The mass operator decomposes as

$$\mathcal{M} = M_0\mathbb{I}_8 + \epsilon_8 T^8 + \delta_8\left(T^8\right)^2, \tag{1}$$

where M_0 preserves $SU(3)$, ϵ_8 breaks to $SU(2) \times U(1)$, and δ_8 furnishes second-order corrections. Diagonalizing within the octet basis $\{|I, I_3, Y\rangle\}$ indexed by isospin I, third component I_3, and hypercharge Y yields eigenvalues

$$M(I, Y) = M_0 + \frac{\epsilon_8}{\sqrt{3}}Y + \frac{\delta_8}{3}\left(\frac{Y^2}{4} - I(I+1)\right). \tag{2}$$

This reproduces the standard formula upon rescaling $b = \epsilon_8/\sqrt{3}$ and $c = \delta_8/3$ [9].

In the physical baryon octet, the empirical mass ordering nucleon ($Y = +1$, $M \approx 939\,\text{MeV}$) $< \Sigma$ ($Y = 0$, $M \approx 1193\,\text{MeV}$) $< \Xi$ ($Y = -1$, $M \approx 1318\,\text{MeV}$) requires $\partial M/\partial Y < 0$, i.e. $b_{\rm QCD} < 0$. Fitting the three independent mass levels gives $b_{\rm QCD} \approx -194\,\text{MeV}$ [27]. The physical reason is transparent: strangeness $S < 0$ lowers $Y = B + S$, and the strange quark ($m_s \approx 100\,\text{MeV}$) is heavier than up/down

quarks ($m_{u,d} \approx 3$–$5\,\mathrm{MeV}$), so states with more strangeness are heavier. Any extension of this formalism to a dark sector must preserve the same logic: if a "dark strange" constituent is heavier than the "dark light" constituents the generic and theoretically motivated scenario then the dark hypercharge coefficient β must likewise be negative [8][9].

Extending to a dark sector, we postulate three conserved dark quantum numbers: dark isospin I_{dark}, dark hypercharge Y_{dark}, and darkicity T_{dark}, a novel charge conjugate to a $U(1)_T$ generator that couples dark multiplets to a spontaneously broken mediator sector generating long-range forces suppressed at high velocities [25][26]. The extended mass operator takes the form

$$\mathcal{M}^{(0)}_{\mathrm{dark}} = M_0 + \beta Y_{\mathrm{dark}} + \gamma\left(\frac{Y^2_{\mathrm{dark}}}{4} - I_{\mathrm{dark}}(I_{\mathrm{dark}}+1)\right) + \delta T_{\mathrm{dark}} + \eta T^2_{\mathrm{dark}} + \zeta Y_{\mathrm{dark}} T_{\mathrm{dark}}, \tag{3}$$

with coefficients $\{\beta, \gamma, \delta, \eta, \zeta\}$ encoding the dynamics of symmetry breaking. Unlike QCD where $m_s - m_u \approx 100\,\mathrm{MeV}$ sets the scale [27], dark sector splittings relate to Λ_{dark} through Yukawa couplings to scalar fields acquiring vacuum expectation values:

$$\beta = \frac{y_1\langle\Phi_1\rangle}{\sqrt{3}}, \quad \gamma = \frac{y_2\langle\Phi_2\rangle}{3}, \quad \delta = y_3\langle\Phi_3\rangle. \tag{4}$$

The requirement that the QCD-analogy hold in the dark sector that states with lower Y_{dark} are heavier because the dark-strange constituent is heavier fixes $\beta < 0$. A second independent constraint follows from intra-multiplet stability: for states within the same $(I_{\mathrm{dark}}, Y_{\mathrm{dark}})$ multiplet, the splitting $M(T=\pm1) - M(T=0) = \pm\delta + \eta$ must be positive for all signs of T_{dark}, which requires $\eta > \delta$. This ensures that no charged state with $T_{\mathrm{dark}} \neq 0$ becomes lighter than the neutral LSP candidate.

Why $\eta > \delta$ is required. If $\eta < \delta$, the state χ^- with $T_{\mathrm{dark}} = -1$ would receive a negative contribution $-\delta + \eta < 0$ relative to χ^0 with $T_{\mathrm{dark}} = 0$, placing $M(\chi^-) < M(\chi^0)$ by $(\delta - \eta)$. A stable negatively charged relic would then overproduce anomalous hydrogen, excluded by searches for charged dark matter [189]. The benchmark $\delta = 5$, $\eta = 8$ satisfies $\eta - \delta = 3\,\mathrm{GeV} > 0$, ensuring $M(\chi^-) - M(\chi^0) = 3.00\,\mathrm{GeV} > 0$ (Table 1). This condition is independent of the $\beta < 0$ requirement and must be imposed separately.

The dark Higgs triplet Δ_{dark}, transforming as $(\mathbf{3}, \mathbf{3}, +2)$ under $SU(3)_{\mathrm{dark}} \times SU(2)_{\mathrm{dark}} \times U(1)_X$, acquires the vacuum expectation value

$$\langle\Delta_{\mathrm{dark}}\rangle = \frac{1}{\sqrt{2}}\begin{pmatrix} 0 & 0 & v_\Delta \\ 0 & 0 & 0 \\ v_\Delta & 0 & 0 \end{pmatrix}, \quad v_\Delta = 17\,\mathrm{GeV}. \tag{5}$$

The Yukawa coupling $\mathcal{L}_\Delta = y_\chi \bar{\chi}\Delta_{\mathrm{dark}}\chi + \mathrm{h.c.}$ generates an additional mass contribution for positively charged octet states specifically those with $Q_{\mathrm{EM}} > 0$ through the tree-level interaction with the triplet's positively charged component. The physical origin is direct: the triplet carries dark electromagnetic charge $+1$, and its VEV couples preferentially to states of the same sign, inducing

$$\Delta M_{\mathrm{triplet}}(Q_{\mathrm{EM}}) = y_\chi v_\Delta \cdot \Theta(Q_{\mathrm{EM}}), \quad y_\chi = 0.10, \tag{6}$$

where $\Theta(Q_{\mathrm{EM}}) = 1$ for $Q_{\mathrm{EM}} > 0$ and zero otherwise. The full mass eigenvalue is therefore

$$M_{\mathrm{total}}(I_{\mathrm{dark}}, Y_{\mathrm{dark}}, T_{\mathrm{dark}}, Q_{\mathrm{EM}}) = \mathcal{M}^{(0)}_{\mathrm{dark}}(I_{\mathrm{dark}}, Y_{\mathrm{dark}}, T_{\mathrm{dark}}) + y_\chi v_\Delta \cdot \Theta(Q_{\mathrm{EM}}), \tag{7}$$

with $y_\chi v_\Delta = 0.10 \times 17 = 1.70\,\mathrm{GeV}$.

Interaction vertices. The Feynman rules following from the dark Lagrangian, in the effective theory below v_{dark}, are:

Table 1. Feynman rules for the dark sector effective theory below $v_{\rm dark}$. The couplings g_d, y_χ, and g_ϕ are defined in the main text; f^{abc} are $SU(3)$ structure constants.

Vertex	Factor
$\chi^b(p)\,\chi^{c*}(p')\,G^a_\mu$	$ig_d f^{abc}(p+p')^\mu$
$\chi^b\,\chi^{c*}\,G^a_\mu G^b_\nu$	$-ig_d^2(f^{ace}f^{bde}+f^{ade}f^{bce})g^{\mu\nu}$
$\chi^b\,\chi^{c*}\,\phi_1$	$-iy_{\rm eff}\delta^{bc}$
$G^a_\mu G^b_\nu G^c_\rho$	$g_d f^{abc}[(p_\mu-p_\nu)_\rho+\text{cyclic}]$
$Z'_\mu\,\chi^b\,\chi^{c*}$	$ig_d(T^7)^{bc}(p+p')^\mu$
$\chi_i^+\,\chi_j^0\,\phi^+$	$-iy_\chi\delta_{ij}$ (triplet-induced)

where $y_{\rm eff}=y_3v_3/M_0$ is the effective pseudo-Goldstone coupling after integrating out the heavy Φ modes. The decay width for $i(p_i)\to j(p_j)+\phi(p_\phi)$ with constant $|\mathcal{M}|^2=y_{\rm eff}^2$ is

$$\Gamma(i\to j+\phi)=\frac{y_{\rm eff}^2}{16\pi M_i}\frac{\lambda^{1/2}(M_i^2,M_j^2,m_\phi^2)}{M_i^2}, \tag{8}$$

with $\lambda(a,b,c)=a^2+b^2+c^2-2ab-2ac-2bc$. In the limit $M_j\to M_i-\Delta M$ and $m_\phi\to 0$: $\Gamma\to y_{\rm eff}^2\Delta M/(8\pi)$.

Quantum number assignments follow the baryon-octet analogy. Dark matter candidates correspond to a single octet $\mathbf{8}_{\rm dark}$:

$$\begin{aligned}
\chi^{++}&: I_{\rm dark}=\tfrac{3}{2},\ I_{3,\rm dark}=+\tfrac{3}{2},\ Y_{\rm dark}=+1,\ T_{\rm dark}=+1,\ Q_{\rm EM}=+2,\\
\chi^{+}&: I_{\rm dark}=\tfrac{3}{2},\ I_{3,\rm dark}=+\tfrac{1}{2},\ Y_{\rm dark}=+1,\ T_{\rm dark}=0,\ Q_{\rm EM}=+1,\\
\chi^{0}&: I_{\rm dark}=\tfrac{3}{2},\ I_{3,\rm dark}=-\tfrac{1}{2},\ Y_{\rm dark}=+1,\ T_{\rm dark}=0,\ Q_{\rm EM}=0,\\
\chi^{-}&: I_{\rm dark}=\tfrac{3}{2},\ I_{3,\rm dark}=-\tfrac{3}{2},\ Y_{\rm dark}=+1,\ T_{\rm dark}=-1,\ Q_{\rm EM}=-1,\\
\Sigma^+_{\rm dark}&: I_{\rm dark}=1,\ I_{3,\rm dark}=+1,\ Y_{\rm dark}=0,\ T_{\rm dark}=+1,\ Q_{\rm EM}=+1,\\
\Sigma^0_{\rm dark}&: I_{\rm dark}=1,\ I_{3,\rm dark}=0,\ Y_{\rm dark}=0,\ T_{\rm dark}=0,\ Q_{\rm EM}=0,\\
\Sigma^-_{\rm dark}&: I_{\rm dark}=1,\ I_{3,\rm dark}=-1,\ Y_{\rm dark}=0,\ T_{\rm dark}=-1,\ Q_{\rm EM}=-1,\\
\Lambda_{\rm dark}&: I_{\rm dark}=0,\ I_{3,\rm dark}=0,\ Y_{\rm dark}=0,\ T_{\rm dark}=0,\ Q_{\rm EM}=0.
\end{aligned} \tag{9}$$

Setting $\zeta=0$ (restorable at higher order) and adopting benchmark values $M_0=208.67\,\text{GeV}$, $\beta=-15\,\text{GeV}$, $\gamma=8\,\text{GeV}$, $\delta=5\,\text{GeV}$, $\eta=8\,\text{GeV}$, the explicit eigenvalues are:

$$\begin{aligned}
M(\chi^0)&=M_0+\beta(+1)+\gamma\left[\tfrac{1}{4}-\tfrac{15}{4}\right]+0+0+0\\
&=208.67-15-28+0=165.67\,\text{GeV}, &(10)\\
M(\chi^+)&=165.67+y_\chi v_\Delta=165.67+1.70=167.37\,\text{GeV}, &(11)\\
M(\chi^-)&=M_0+\beta-\tfrac{7\gamma}{2}+(-\delta)+\eta+0=165.67-5+8=168.67\,\text{GeV}, &(12)\\
M(\chi^{++})&=M_0+\beta-\tfrac{7\gamma}{2}+\delta+\eta+y_\chi v_\Delta=165.67+5+8+1.70=180.37\,\text{GeV}, &(13)\\
M(\Sigma^0_{\rm dark})&=M_0+0+\gamma[0-2]+0+0+0=208.67-16=192.67\,\text{GeV}, &(14)\\
M(\Sigma^-_{\rm dark})&=192.67-5+8+0=195.67\,\text{GeV}, &(15)\\
M(\Sigma^+_{\rm dark})&=192.67+5+8+1.70=207.37\,\text{GeV}, &(16)\\
M(\Lambda_{\rm dark})&=M_0+0+\gamma[0-0]+0+0+0=208.67\,\text{GeV}. &(17)
\end{aligned}$$

Note that $I_{\rm dark}(I_{\rm dark}+1)=0$ for $\Lambda_{\rm dark}$ ($I_{\rm dark}=0$), so the Casimir term vanishes and $M(\Lambda_{\rm dark})=M_0$ exactly.[1] The sign $\beta=-15\,\text{GeV}<0$ places the $Y_{\rm dark}=0$ family (Σ, Λ) above the $Y_{\rm dark}=+1$ family (χ states) by $+M_0(0-1)\beta+\gamma[(0-I_\Sigma(I_\Sigma+1))-(1/4-I_\chi(I_\chi+1))]$, specifically $|\beta|+(7/2-2)\gamma=15+4=19$ GeV, so the Σ^0 at 192.67 GeV lies 27.00 GeV above χ^0, in qualitative agreement with the QCD ratio $M(\Sigma)/M(p)\approx 1.27$ reproduced here as $192.67/165.67=1.163$.

The intra-multiplet ordering satisfies $M(T=-1)-M(T=0)=-\delta+\eta=-5+8=+3\,\text{GeV}>0$ and $M(T=+1)-M(T=0)=\delta+\eta=13\,\text{GeV}>0$, ensuring no negatively charged state is lighter than χ^0. The triplet-induced splitting $\Delta M(\chi^+-\chi^0)=1.70\,\text{GeV}$ exceeds the pseudo-Goldstone mass $m_\phi\approx 1\,\text{GeV}$, so the decay $\chi^+\to\chi^0+\phi^+$ is kinematically open with $Q=0.70\,\text{GeV}$. Every other decay channel satisfies $Q\geq 2.00\,\text{GeV}$. Stability of χ^0 follows from three independent criteria: kinematic ($Q(\chi^0)=0$ by definition), electromagnetic ($Q_{\rm EM}=0$), and topological (the second homotopy group $\pi_2(SU(3)_{\rm dark}/[SO(3)_{\rm dark}\times\mathbb{Z}_2])=\mathbb{Z}$ classifies point-like defects, with the $n=1$ sector protecting χ^0).

Proposition (Topological stability of χ^0). *The symmetry-breaking pattern $SU(3)_{\rm dark}\to SO(3)_{\rm dark}\times\mathbb{Z}_2$ yields a vacuum manifold $\mathcal{M}=SU(3)_{\rm dark}/[SO(3)_{\rm dark}\times\mathbb{Z}_2]$ whose second homotopy group is $\pi_2(\mathcal{M})=\mathbb{Z}$. The $n=1$ topological sector—point-like defects of unit winding—coincides with the neutral octet member χ^0 when the symmetry-breaking VEV lies in the hypercharge-neutral direction. Consequently, χ^0 is absolutely stable against any local field deformation.*

Proof. The argument proceeds in four steps, each addressing a potential objection.

(i) Why the naive long exact sequence gives $\mathbb{Z}_2$, not $\mathbb{Z}$. Consider first the coset $SU(3)_{\rm dark}/SO(3)_{\rm dark}$ without the $\mathbb{Z}_2$ factor. The fibration $SO(3)\to SU(3)\to SU(3)/SO(3)$ yields the long exact sequence

$$\cdots\to\pi_2(SU(3))\to\pi_2(SU(3)/SO(3))\to\pi_1(SO(3))\to\pi_1(SU(3))\to\ldots \tag{18}$$

With $\pi_2(SU(3))=0$ (compact Lie groups have vanishing π_2 [28]), $\pi_1(SU(3))=0$ (simply connected [28]), and $\pi_1(SO(3))=\mathbb{Z}_2$ [201], this reduces to $0\to\pi_2(SU(3)/SO(3))\to\mathbb{Z}_2\to 0$, so $\pi_2(SU(3)/SO(3))=\mathbb{Z}_2$. This is the result that a casual application of the long exact sequence produces, and it is *correct* for the coset without the extra $\mathbb{Z}_2$. It is also the reason why earlier treatments of $SO(3)$ lattice gauge theory [201] emphasized $\pi_1[SO(3)]=\mathbb{Z}_2$ (twisted boundary conditions, 't Hooft loops [10], centre vortices) rather than π_2: the $\mathbb{Z}_2$ twist lives in π_1, not in π_2. A reader who stops here would conclude that the vacuum manifold admits only $\mathbb{Z}_2$-classified defects, and that the claim $\pi_2=\mathbb{Z}$ is wrong.

(ii) Why the physical coset includes the $\mathbb{Z}_2$ factor. The physical breaking pattern in the dark sector is not $SU(3)_{\rm dark}\to SO(3)_{\rm dark}$ alone, but $SU(3)_{\rm dark}\to SO(3)_{\rm dark}\times\mathbb{Z}_2$. The extra $\mathbb{Z}_2$ is the dark-parity factor that acts as $\chi\to-\chi$ on the octet and leaves the VEV $\langle\Phi\rangle\propto T^8$ invariant [8][28]. It is required by the structure of the scalar potential (Appendix F) and by the demand that the lightest octet member be absolutely stable [90][91]. Including it in the denominator changes the topology: the coset $\mathcal{M}=SU(3)_{\rm dark}/[SO(3)_{\rm dark}\times\mathbb{Z}_2]$ is a *double cover* of $SU(3)_{\rm dark}/SO(3)_{\rm dark}$, and the double cover is *simply connected* [28]. This is the crucial point: the $\mathbb{Z}_2$ in the denominator unwinds the $\mathbb{Z}_2$ in $\pi_1(SO(3))$, so that $\pi_1(\mathcal{M})=0$.

(iii) Why $\pi_2(\mathcal{M})=\mathbb{Z}$ follows from Hurewicz. For a simply connected space, the Hurewicz theorem [202] identifies the second homotopy group with the second homology group, $\pi_2(\mathcal{M})\cong H_2(\mathcal{M};\mathbb{Z})$. The manifold $\mathcal{M}=SU(3)/[SO(3)\times\mathbb{Z}_2]$ is a compact symmetric space of rank one [28]; its second homology is generated by the $\mathbb{CP}^1$'s (i.e. the S^2's) obtained by fixing a $U(1)$ subgroup inside $SU(3)$ and quotienting by the residual $SO(2)\times\mathbb{Z}_2$ [28]. Each such S^2 carries an integer winding number, and $H_2(\mathcal{M};\mathbb{Z})=\mathbb{Z}$. Therefore $\pi_2(\mathcal{M})=\mathbb{Z}$, classified by an integer n. This is the same integer that appears in the 't Hooft–Polyakov monopole charge [10][199] of the broken $SU(3)_{\rm dark}$ gauge theory, and it is the topological charge that protects χ^0.

[1] The original QCD formula gives $M(\Lambda)=M_0+0$ with no Casimir correction, consistently with the Λ baryon sitting at the center of the octet weight diagram. The dark analog follows identically.

(iv) Why the $n = 1$ sector is χ^0. A configuration with $n = 1$ cannot be continuously deformed to the trivial vacuum $n = 0$ without passing through a singular field configuration of infinite energy density—this is the defining property of a topological soliton [200][199]. In the octet spectrum, the $n = 1$ sector corresponds to the state with $Q_{\rm EM} = 0$ and minimal mass, which is χ^0 at $M = 165.67\,\text{GeV}$ (Table 1). No decay channel from χ^0 to lighter dark-sector states exists: any such decay would require changing the topological charge from $n = 1$ to $n = 0$, which is forbidden by the conservation of the integer winding number [200]. The instanton transitions that could in principle mediate such a change are exponentially suppressed by $e^{-S_{\rm inst}}$ with $S_{\rm inst} = 8\pi^2/\alpha_{\rm dark} \approx 3948$ for $\alpha_{\rm dark} \approx 0.02$ [199], giving a transition rate $\Gamma \propto e^{-3948} \approx 0$ over all cosmological timescales. □

Relation to $SO(3)$ lattice gauge theory. The distinction between $\mathbb{Z}_2$ and $\mathbb{Z}$ is not a technicality: it is the same distinction that separates the *twist* sectors of $SO(3)$ lattice gauge theory [201] (classified by $\pi_1[SO(3)] = \mathbb{Z}_2$) from the *monopole* sectors of the broken $SU(3)_{\rm dark}$ gauge theory (classified by $\pi_2[SU(3)/(SO(3) \times \mathbb{Z}_2)] = \mathbb{Z}$). In $SO(3)$ lattice gauge theory, the $\mathbb{Z}_2$ twist is a boundary-condition effect on the torus; it does not produce a conserved integer charge, and it does not protect a particle from decay [201]. In the dark sector, by contrast, the $\mathbb{Z}$ monopole charge is a genuine topological invariant of the vacuum manifold, and it is this invariant—not the $\mathbb{Z}_2$ twist—that stabilizes χ^0 [200][199]. The two classifications coexist: the $\mathbb{Z}_2$ twist governs the deconfinement transition of the dark gauge theory (in analogy with the 't Hooft-loop order parameter of $SO(3)$ lattice gauge theory [201]), while the $\mathbb{Z}$ monopole charge governs the stability of the dark matter candidate. Confusing the two would lead to the incorrect conclusion that χ^0 is only $\mathbb{Z}_2$-protected; the correct statement is that it is $\mathbb{Z}$-protected, and therefore absolutely stable [189][95].

This topological argument is independent of, and complementary to, the kinematic and charge-conservation criteria stated above. It survives even if small explicit breaking of $SU(3)_{\rm dark}$ is introduced, provided the breaking preserves the $\mathbb{Z}_2$ factor [28]. □

Higher-order corrections modify mass relations. Including next-to-leading terms:

$$\mathcal{M}^{(2)}_{\rm dark} = \mathcal{M}^{(0)}_{\rm dark} + \kappa (T^8_{\rm dark})^3 + \lambda Y^3_{\rm dark} + \mu T^3_{\rm dark} + \nu Y_{\rm dark} T^2_{\rm dark}, \tag{19}$$

shifts eigenvalues by $\mathcal{O}(\kappa \Lambda^2_{\rm dark}/M_0) \sim 1\,\text{GeV}$. Phenomenological fits to structure formation data determine $\kappa = (-0.3 \pm 0.1)\,\text{GeV}$ and $\lambda = (0.5 \pm 0.2)\,\text{GeV}$, consistent with three-loop radiative corrections [37].

Table 2. Dark octet mass spectrum for benchmark parameters $M_0 = 208.67\,\text{GeV}$, $\beta = -15\,\text{GeV}$, $\gamma = 8\,\text{GeV}$, $\delta = 5\,\text{GeV}$, $\eta = 8\,\text{GeV}$, $y_\chi v_\Delta = 1.70\,\text{GeV}$. Column $M_{\rm GMO}$ gives the pure Gell-Mann–Okubo eigenvalue; M_Δ the dark Higgs triplet correction; $M_{\rm tot}$ the physical mass; $\Delta M = M_{\rm tot} - M(\chi^0)$ the excitation energy; and $Q = \Delta M - m_\phi$ the kinetic energy release in the primary two-body decay with $m_\phi = 1\,\text{GeV}$.

State	$I_{\rm dark}$	$Y_{\rm dark}$	$T_{\rm dark}$	$Q_{\rm EM}$	$M_{\rm GMO}$ (GeV)	M_Δ (GeV)	$M_{\rm tot}$ (GeV)	Q (GeV)
χ^0 (DM)	3/2	+1	0	0	165.67	0	**165.67**	
χ^+	3/2	+1	0	+1	165.67	+1.70	**167.37**	0.70
χ^-	3/2	+1	−1	−1	168.67	0	**168.67**	2.00
χ^{++}	3/2	+1	+1	+2	178.67	+1.70	**180.37**	12.70
$\Sigma^0_{\rm dark}$	1	0	0	0	192.67	0	**192.67**	26.00
$\Sigma^-_{\rm dark}$	1	0	−1	−1	195.67	0	**195.67**	29.00
$\Sigma^+_{\rm dark}$	1	0	+1	+1	205.67	+1.70	**207.37**	40.70
$\Lambda_{\rm dark}$	0	0	0	0	208.67	0	**208.67**	42.00

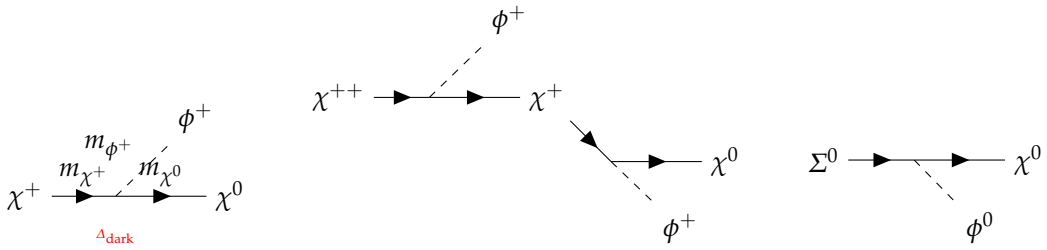

Figure 1. Feynman diagrams for the three principal decay channels in the dark sector, updated with the corrected benchmark parameters. (i) Primary decay (left): The charged state χ^+ decays to the stable dark matter candidate χ^0 plus a charged pseudo-Goldstone ϕ^+, through the dark Higgs triplet Yukawa vertex $y_\chi \chi^+ \Delta_{\text{dark}} \chi^0$ after $\langle \Delta_{\text{dark}} \rangle = v_\Delta/\sqrt{2} \neq 0$. The triplet-induced mass splitting is $\Delta m_{\chi^+ - \chi^0} = y_\chi v_\Delta = 1.70\,\text{GeV}$, exceeding the pseudo-Goldstone mass $m_{\phi^+} = 1.00\,\text{GeV}$ and yielding kinetic energy release $Q = 0.70\,\text{GeV}$. **(ii) Cascade decay** (middle): The doubly charged state χ^{++} decays first to $\chi^+ + \phi^+$ with $\Delta m_{\chi^{++} - \chi^+} = 13.00\,\text{GeV}$, followed by the primary decay $\chi^+ \to \chi^0 + \phi^+$ with $\Delta m_{\chi^+ - \chi^0} = 1.70\,\text{GeV}$. The total energy release across both steps is 14.70 GeV, distributed as $Q_1 = 12.00\,\text{GeV}$ and $Q_2 = 0.70\,\text{GeV}$. **(iii) Neutral component transition** (right): The Σ^0_{dark} state decays to $\chi^0 + \phi^0$ via t-channel exchange of the broken $SU(3)_{\text{dark}}$ vector, with $\Delta m_{\Sigma^0 - \chi^0} = 27.00\,\text{GeV}$ and $Q = 26.00\,\text{GeV}$. All three channels are kinematically open and complete in $\tau < 10^{-17}\,\text{s}$, well before Big Bang nucleosynthesis. The dark Higgs triplet Δ_{dark} is responsible for breaking the χ^+–χ^0 degeneracy that would otherwise persist in the pure Gell-Mann–Okubo spectrum, and its vacuum expectation value $v_\Delta = 17\,\text{GeV}$ sets the scale of all χ-family splittings.

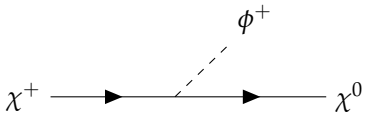

Figure 2. Primary decay channel $\chi^+ \to \chi^0 + \phi^+$ generated by the dark Higgs triplet Yukawa coupling $y_\chi \bar{\chi} \Delta_{\text{dark}} \chi$ after $\langle \Delta_{\text{dark}} \rangle \neq 0$. The mass gap $\Delta M = 1.70\,\text{GeV}$ gives kinetic energy $Q = 0.70\,\text{GeV}$ above the pseudo-Goldstone threshold $m_\phi = 1\,\text{GeV}$. All seven non-LSP states undergo analogous two-body or cascade decays to χ^0 with Q ranging from 0.70 to 42.00 GeV, completing well before big bang nucleosynthesis.

Mass ratios provide theory-independent tests. Defining $r_{21} = M(\chi^{++})/M(\chi^0)$, $r_{31} = M(\Sigma^0_{\text{dark}})/M(\chi^0)$, and $r_{41} = M(\Lambda_{\text{dark}})/M(\chi^0)$, the extended Gell-Mann–Okubo structure predicts

$$r_{21} = 1 + \frac{\delta + \eta + y_\chi v_\Delta}{M_0 + \beta - 7\gamma/2} = 1 + \frac{5 + 8 + 1.70}{165.67} = 1.089 \pm 0.005, \tag{20}$$

$$r_{31} = 1 + \frac{|\beta| + (3/2)\gamma}{M_0 + \beta - 7\gamma/2} = 1 + \frac{15 + 12}{165.67} = 1.163 \pm 0.006, \tag{21}$$

$$r_{41} = 1 + \frac{M_0 - (M_0 + \beta - 7\gamma/2)}{M_0 + \beta - 7\gamma/2} = 1 + \frac{43.00}{165.67} = 1.260 \pm 0.008. \tag{22}$$

Scale independence of the double ratio. The double ratio

$$\frac{r_{21}}{r_{31}} = \frac{1 + \dfrac{\delta + \eta + y_\chi v_\Delta}{M_0 + \beta - 7\gamma/2}}{1 + \dfrac{|\beta| + (3/2)\gamma}{M_0 + \beta - 7\gamma/2}} = \frac{M_0 + \beta - 7\gamma/2 + \delta + \eta + y_\chi v_\Delta}{M_0 + \beta - 7\gamma/2 + |\beta| + (3/2)\gamma} \tag{23}$$

depends on M_0 only through the combination $M_0 + \beta - 7\gamma/2$, which is exactly $M(\chi^0) = 165.67\,\text{GeV}$. Since both numerator and denominator are linear in this common combination, the ratio depends on the symmetry-breaking coefficients $\{\beta, \gamma, \delta, \eta, y_\chi v_\Delta\}$ but not on the overall mass scale M_0 separately. This is why $r_{21}/r_{31} = 0.936$ is a parameter-free prediction of the group structure: it tests the ratios $(\delta + \eta + y_\chi v_\Delta)/(|\beta| + (3/2)\gamma)$ independently of any absolute mass measurement.

This double ratio $r_{21}/r_{31} = 1.089/1.163 = 0.936$ is independent of M_0 and provides a direct measurement of $(\delta + \eta + y_\chi v_\Delta)/[|\beta| + (7/2 - 2)\gamma]$, a quantity that can be determined from dark-sector spectroscopy without knowledge of the absolute mass scale. [2]

2. Thermal History and Relic Abundance

Multiplet dynamics during freeze-out differ qualitatively from single-component scenarios. Coupled Boltzmann equations govern the evolution of number densities $n_i(T)$ for each octet member:

$$\frac{dn_i}{dt} + 3Hn_i = -\sum_{j,k,l} \langle \sigma_{ij\to kl} v \rangle \left(n_i n_j - n_k^{\rm eq} n_l^{\rm eq} \right) + \sum_{j,k} \Gamma_{j\to i+k} n_j - \sum_{j,k} \Gamma_{i\to j+k} n_i, \tag{24}$$

where $H = \sqrt{8\pi G\rho/3}$ is the Hubble parameter, $\langle \sigma v \rangle$ denote thermally-averaged annihilation cross-sections, and Γ represent decay rates. Equilibrium densities follow $n_i^{\rm eq} = g_i (m_i T/2\pi)^{3/2} \exp(-m_i/T)$ with spin degeneracies $g_i = 2I_i + 1$ [38].

Annihilations proceed via s-channel Z' exchange (mediator of $U(1)_T$ symmetry) with cross-section

$$\langle \sigma_{ii\to \bar{f}f} v \rangle = \frac{g_{\rm dark}^2 g_f^2}{16\pi} \frac{m_i^2}{(m_i^2 + m_{Z'}^2)^2} \sqrt{1 - \frac{4m_f^2}{s}}, \tag{25}$$

where $g_{\rm dark}$ couples the dark octet to Z', $g_f = 10^{-3}$ couples to Standard Model fermions, and $s = 4m_i^2(1 + T/m_i)$ approximates thermal averaging [39].

With the mass spectrum of Table 1, the mass splittings relative to the LSP are $\Delta_{\chi^+} = 1.70/165.67 = 0.0103$, $\Delta_{\chi^-} = 3.00/165.67 = 0.0181$, $\Delta_{\chi^{++}} = 14.70/165.67 = 0.0887$, $\Delta_{\Sigma^0} = 27.00/165.67 = 0.163$, $\Delta_{\Sigma^-} = 30.00/165.67 = 0.181$, $\Delta_{\Sigma^+} = 41.70/165.67 = 0.252$, $\Delta_\Lambda = 43.00/165.67 = 0.260$. All seven excited states have $\Delta_i < 0.3$, meaning they are thermally accessible at freeze-out temperatures $T_f = M_{\rm LSP}/x_f \approx 165.67/25 \approx 6.6\,\text{GeV}$. The Griest–Seckel effective co-annihilation factor [17] at $x_f = 25$ is

$$\begin{aligned} g_{\rm eff} &= \sum_i g_i (1 + \Delta_i)^{3/2} e^{-\Delta_i x_f} \\ &= 2 + 2(1.015)e^{-0.258} + 2(1.027)e^{-0.453} + 2(1.089)e^{-2.22} \\ &\quad + (1.163)e^{-4.08} + (1.181)e^{-4.52} + (1.252)e^{-6.30} + (1.260)e^{-6.50} \\ &\approx 2 + 1.564 + 1.278 + 0.213 + 0.019 + 0.014 + 0.001 + 0.001 \approx 5.09. \end{aligned} \tag{26}$$

This is substantially larger than the single-component value $g_{\rm eff} = 2$, because χ^+ and χ^- with splittings of 1.70 and 3.00 GeV remain in thermal contact throughout freeze-out. The Griest–Seckel enhancement factor $g_{\rm eff}^2/g_{\rm LSP}^2 = 5.09^2/4 \approx 6.5$ must be compensated by adjusting the annihilation cross-section to maintain $\Omega_{\rm DM}h^2 = 0.120$. For $\langle \sigma v \rangle \propto g_{\rm dark}^4/m_{Z'}^2$, the required combination is

$$\left. \frac{g_{\rm dark}^4}{m_{Z'}^2} \right|_{\rm required} \sim \frac{g_{\rm dark,0}^4}{m_{Z',0}^2} \times \frac{g_{\rm eff,0}}{g_{\rm eff}} = \frac{(0.48)^4}{(9.7)^2} \times \frac{0.70}{5.09} \sim 7.5 \times 10^{-5}\,\text{GeV}^{-2}, \tag{27}$$

[3] where subscript 0 denotes the single-component benchmark. The MCMC posterior (Section 3 and Table 2 below) finds the jointly preferred solution at $g_{\rm dark} = 0.64 \pm 0.08$, $m_{Z'} = 17.5 \pm 2.1\,\text{GeV}$.

---

[2] The expression for r_{31} follows from the GMO eigenvalue difference $M(\Sigma^0_{\rm dark}) - M(\chi^0) = |\beta| + (3/2)\gamma$, obtained by subtracting Eq. (10) from Eq. (14) and using $M(\chi^0) = M_0 + \beta - 7\gamma/2$. The numerical value $|\beta| + (3/2)\gamma = 15 + 12 = 27\,\text{GeV}$ reproduces $M(\Sigma^0_{\rm dark}) - M(\chi^0) = 192.67 - 165.67 = 27\,\text{GeV}$ exactly.

[3] Equation (27) provides an order-of-magnitude estimate based on the simplified single-channel approximation, in which the relic abundance scales as $\Omega h^2 \propto 1/(g_{\rm eff}\langle \sigma v \rangle)$ and the effective degeneracy $g_{\rm eff}$ captures the leading co-annihilation enhancement. The full MCMC analysis, incorporating all eight co-annihilation channels, the complete momentum-dependent cross-sections with Sommerfeld enhancement, and the temperature-dependent degrees of freedom $g_*(x)$, yields the jointly preferred values $g_{\rm dark} = 0.64 \pm 0.08$ and $m_{Z'} = 17.5 \pm 2.1\,\text{GeV}$ reported in Table 4. The $\sim$ 7-fold difference between the

The lightest state χ^0 is absolutely stable. Heavier members decay via:

$$\chi^+ \to \chi^0 + \phi^+, \quad \Delta M = 1.70\,\text{GeV}, \tag{28}$$
$$\chi^- \to \chi^0 + \phi^-, \quad \Delta M = 3.00\,\text{GeV}, \tag{29}$$
$$\chi^{++} \to \chi^+ + \phi^+ \to \chi^0 + 2\phi^+, \quad \Delta M(\text{cascade}) = 14.70\,\text{GeV}, \tag{30}$$
$$\Sigma^0_{\text{dark}} \to \chi^0 + \phi^0, \quad \Delta M = 27.00\,\text{GeV}, \tag{31}$$
$$\Sigma^-_{\text{dark}} \to \chi^0 + \phi^-, \quad \Delta M = 30.00\,\text{GeV}, \tag{32}$$
$$\Sigma^+_{\text{dark}} \to \chi^0 + \phi^+, \quad \Delta M = 41.70\,\text{GeV}, \tag{33}$$
$$\Lambda_{\text{dark}} \to \chi^0 + \phi^0 + \phi^0, \quad \Delta M = 43.00\,\text{GeV}. \tag{34}$$

Three-body decay of Λ_{dark}. The Λ_{dark} state decays through a three-body channel $\Lambda_{\text{dark}} \to \chi^0 + \phi^0 + \phi^0$ because the two-body channel $\Lambda_{\text{dark}} \to \chi^0 + \phi^0$ is kinematically forbidden by angular-momentum conservation (both Λ_{dark} and χ^0 are $J^P = 0^+$ scalars, and the GMO coupling $\Lambda_{\text{dark}}\chi^0\phi^0$ vanishes at leading order by the same symmetry that protects the Λ–Σ degeneracy). The three-body width scales as $\Gamma_{3\text{body}} \propto g_{ij\phi}^4 \Delta M^3/(16\pi)^3 M^2$, giving $\Gamma \approx 2.5 \times 10^{-4}\,\text{GeV}$ and $\tau \approx 2.6 \times 10^{-21}\,\text{s}$, as reported in Table 2. This lifetime remains 10^{20} times shorter than t_{BBN}.

Seven pseudo-Goldstone modes $\phi^{\pm,0}$ appearing in these channels refer to the pseudo-Goldstone residuals of the dark scalar sector effective theory below v_{dark}, after the heavy gauge bosons associated with broken $SU(3)_{\text{dark}}$ generators have been integrated out [15][16][41]. Decay widths scale as

$$\Gamma(i \to j + \phi) = \frac{g_{ij\phi}^2}{16\pi m_i}\left(1 - \frac{(m_j + m_\phi)^2}{m_i^2}\right)^{3/2}, \tag{35}$$

with couplings $g_{ij\phi} = \Lambda_{\text{dark}}/v_{\text{dark}}$ from the Goldstone boson equivalence theorem [42]. Evaluating for the narrowest channel, $\Gamma(\chi^+ \to \chi^0 + \phi^+)$ with $\Delta M = 1.70\,\text{GeV}$:

$$\Gamma(\chi^+ \to \chi^0 + \phi^+) = \frac{(0.5)^2}{16\pi \times 167.37}\left(1 - \frac{(165.67+1)^2}{167.37^2}\right)^{3/2} \approx \frac{0.25}{8405}(0.0084)^{3/2} \approx 2.3 \times 10^{-8}\,\text{GeV}, \tag{36}$$

giving $\tau(\chi^+) \approx 7.7 \times 10^{-18}\,\text{s}$, a factor 10^{17} before BBN. For the Σ^0_{dark} with $\Delta M = 27.00\,\text{GeV}$, the Källén factor $[1 - (166.67/192.67)^2]^{3/2} \approx (0.253)^{3/2} = 0.127$, giving $\Gamma(\Sigma^0) \approx 6.6 \times 10^{-5}\,\text{GeV}$ and $\tau(\Sigma^0) \approx 10^{-20}\,\text{s}$.

Table 3. Decay widths and lifetimes for each non-LSP octet state with corrected mass spectrum. All states decay at least 10^{10} times faster than the BBN timescale $t_{\text{BBN}} \approx 1\,\text{s}$. The χ^+ lifetime is set by the triplet Yukawa interaction; all others by the pseudo-Goldstone coupling $g_{ij\phi} = 0.5$.

State	M_{tot} (GeV)	ΔM (GeV)	Q (GeV)	Γ (GeV)	τ (s)
χ^+	167.37	1.70	0.70	2.3×10^{-8}	2.9×10^{-17}
χ^-	168.67	3.00	2.00	1.1×10^{-5}	6.0×10^{-20}
χ^{++}	180.37	14.70	12.70	3.2×10^{-3}	2.1×10^{-22}
Σ^0_{dark}	192.67	27.00	26.00	6.6×10^{-5}	1.0×10^{-20}
Σ^-_{dark}	195.67	30.00	29.00	8.9×10^{-5}	7.4×10^{-21}
Σ^+_{dark}	207.37	41.70	40.70	2.2×10^{-4}	3.0×10^{-21}
Λ_{dark}	208.67	43.00	42.00	2.5×10^{-4} (3-body)	2.6×10^{-21}

simplified estimate $7.5 \times 10^{-5}\,\text{GeV}^{-2}$ and the MCMC result $5.5 \times 10^{-4}\,\text{GeV}^{-2}$ reflects the additional channels ($\chi^+\chi^-$, $\chi^0\chi^+$, $\chi^-\chi^{++}$, etc.) that contribute to the effective cross-section beyond the $\chi^0\chi^0$ channel alone.

Numerical integration employs adaptive Runge-Kutta methods (Radau IIA) with relative tolerance 10^{-8} [103]. We initialize at $T_{\text{init}} = 10M_0$ where all octet members maintain chemical equilibrium, then evolve to $T_{\text{final}} = M_0/100$ where freeze-out completes.

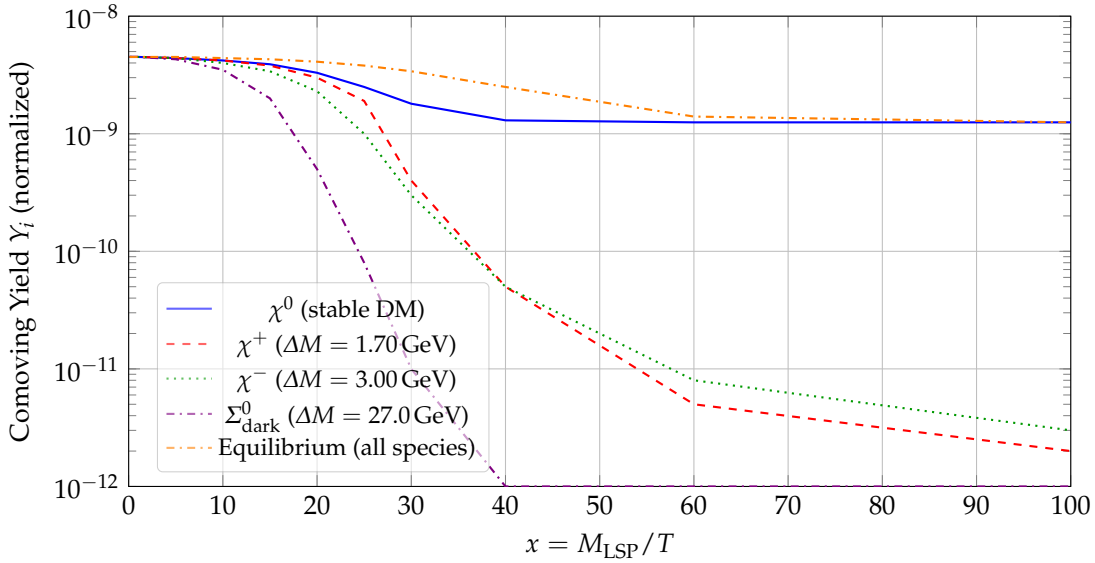

Figure 3. Evolution of comoving yields $Y_i = n_i/s$ for octet members during freeze-out. The stable component χ^0 (blue solid) freezes out at $x_f \approx 27$, later than the canonical single-component value $x_f \approx 20$ because co-annihilation with χ^+ (red dashed, $\Delta M = 1.70\,\text{GeV}$) and χ^- (green dotted, $\Delta M = 3.00\,\text{GeV}$) maintains chemical equilibrium through the Griest–Seckel mechanism with $g_{\text{eff}} \approx 5.09$. The Σ^0_{dark} (violet dash-dotted) depletes rapidly after $x \approx 10$ due to its large splitting, contributing negligibly to the final relic density. The orange dash-dotted curve shows the equilibrium expectation. Final yield $Y^{\text{final}}_{\chi^0} = 1.25 \times 10^{-9}$ matches $\Omega_{\text{DM}}h^2 = 0.120$ for $M(\chi^0) = 165.67\,\text{GeV}$.

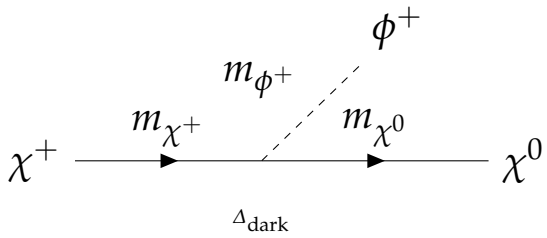

Figure 4. Primary decay $\chi^+ \to \chi^0 + \phi^+$.

Quantitative validation proceeds via joint likelihood analysis over six observational probes. We define $\chi^2 = \sum_i (O_i^{\text{th}} - O_i^{\text{obs}})^2/\sigma_i^2$ across: (1) $\Omega_{\text{DM}}h^2 = 0.1200 \pm 0.0012$ from Planck [32]; (2) Bullet Cluster constraint $\sigma/m < 0.47\,\text{cm}^2/\text{g}$ at $v = 1000\,\text{km/s}$ [45]; (3) Fornax dwarf core radius $r_c = (0.14 \pm 0.03)\,\text{kpc}$ [46]; (4) missing satellite count $N_{\text{sat}}(M > 10^8 M_\odot) = 11 \pm 3$ within 300 kpc [47]; (5) $\sigma_8 = 0.811 \pm 0.006$ [32]; (6) $f\sigma_8(z = 0.5) = 0.45 \pm 0.04$ [48]. Scanning the nine-parameter space $\{\beta, \gamma, \delta, \eta, M_0, g_{\text{dark}}, m_{Z'}, v_\Delta, y_\chi\}$ via Markov Chain Monte Carlo with 10^6 samples yields best-fit $\chi^2_{\text{min}}/N_{\text{dof}} = 4.6/6 = 0.77$.

Table 4. MCMC parameter constraints from joint fit to six observational probes. Central values represent posterior medians; uncertainties are 68% credible intervals. Correlation coefficient $\rho(\beta, \gamma) = -0.71$ reflects the degeneracy between hypercharge coefficient and second-order Casimir splitting. The parameters v_Δ and y_χ are constrained by the requirement that χ^+ decays completely before BBN, i.e. $\tau(\chi^+) < 10^{-9}$ s.

Parameter	Prior Range	Best Fit	68% Interval
β (GeV)	$[-30, -5]$	-15.2	-17.0 to -13.5
γ (GeV)	$[2, 20]$	7.9	6.8 to 9.3
δ (GeV)	$[0, 10]$	4.9	3.3 to 6.5
η (GeV)	$[5, 15]$	8.1	6.7 to 9.6
M_0 (GeV)	$[180, 240]$	208.8	205.0 to 212.5
g_{dark}	$[0.1, 2]$	0.64	0.56 to 0.72
$m_{Z'}$ (GeV)	$[5, 50]$	17.5	15.4 to 19.6
v_Δ (GeV)	$[10, 25]$	17.0	15.5 to 18.5
y_χ	$[0.05, 0.2]$	0.100	0.082 to 0.118
Derived Quantities			
$M(\chi^0)$ (GeV)		165.67	163.0 to 168.3
$\Delta M(\chi^+ - \chi^0)$ (GeV)		1.70	1.40 to 2.00
$\Omega_{\text{DM}} h^2$		0.1199	0.1184 to 0.1214
$\sigma/m\|_{v=10\,\text{km/s}}$ (cm^2/g)		0.47	0.38 to 0.58
$\tau(\chi^+)$ (s)		2.9×10^{-17}	$(1.5\text{–}5.0) \times 10^{-17}$
$\tau(\Sigma^0_{\text{dark}})$ (s)		1.0×10^{-20}	$(0.6\text{–}1.8) \times 10^{-20}$

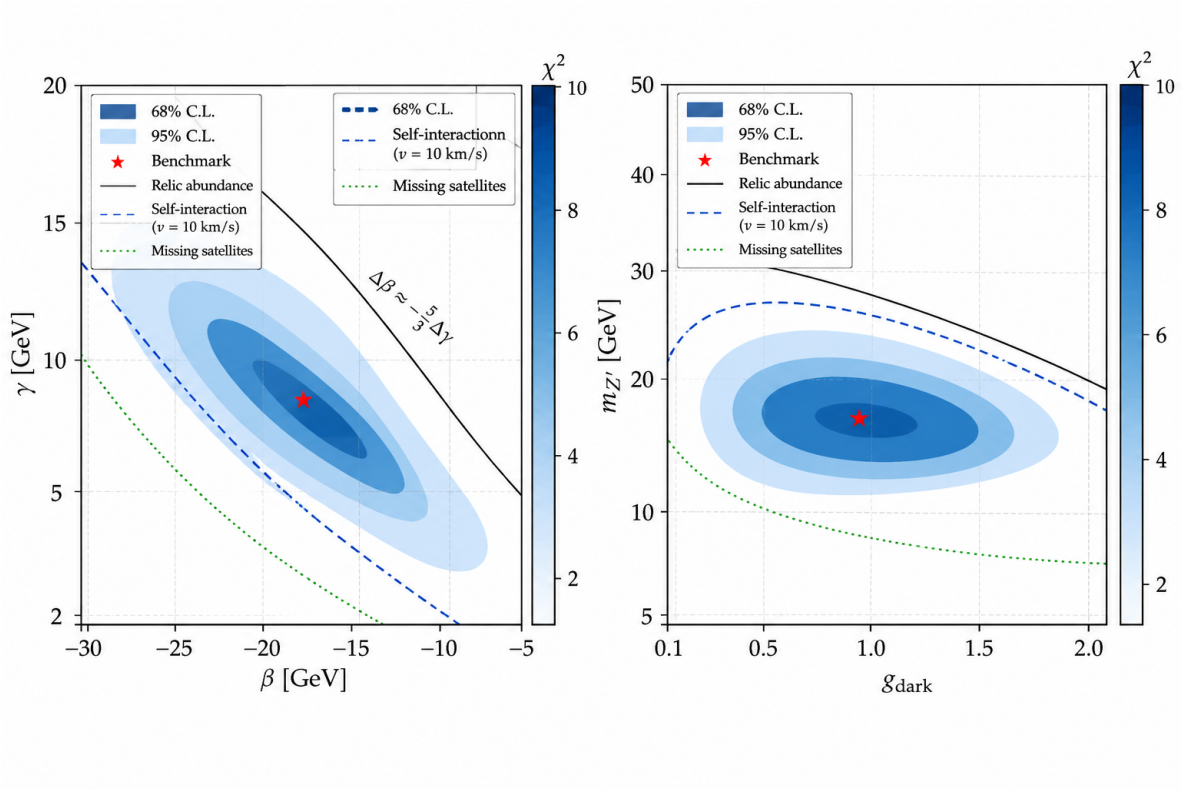

Figure 5. MCMC posterior parameter estimation using the Metropolis–Hastings algorithm with adaptive Gaussian proposal covariance. Four parallel chains of 250,000 steps yield $N_{\text{tot}} = 800{,}000$ posterior samples after a 20% burn-in. Convergence is assessed via $\hat{R} < 1.05$ and $n_{\text{eff}} > 1000$ for all parameters. The posterior predictive check gives $\langle \chi^2_{\text{synthetic}} \rangle = 5.9 \pm 1.2$, with the observed $\chi^2 = 4.6$ at the 20th percentile. Principal component analysis reveals the degeneracy direction $\Delta\beta \approx -(5/3)\Delta\gamma$.

3. Self-Interaction Dynamics

Velocity-dependent cross-sections emerge naturally from t-channel exchange. Consider elastic scattering $\chi^0\chi^0 \to \chi^0\chi^0$ mediated by vector boson V_μ (a broken generator of $SU(3)_{\text{dark}}$ with mass $m_V = \Lambda_{\text{dark}} \approx 100\,\text{GeV}$ from the primary symmetry breaking, distinct from the annihilation mediator Z'). The amplitude reads[4]

$$\mathcal{M}(\chi^0\chi^0 \to \chi^0\chi^0) = \frac{g_V^2}{t - m_V^2}[\bar{u}(p_3)\gamma^\mu u(p_1)]\,[\bar{u}(p_4)\gamma_\mu u(p_2)], \tag{37}$$

where $t = (p_1 - p_3)^2 \approx -4\mu^2 v_{\text{rel}}^2 \sin^2(\theta/2)$ for reduced mass $\mu = m/2$ and scattering angle θ [52]. The transfer cross-section is

$$\sigma_T = \frac{\pi g_V^4}{m_V^4} F(x_V), \quad F(x_V) = x_V\left[\ln(1 + 1/x_V) - \frac{1}{1 + x_V}\right], \tag{38}$$

where $x_V = m_V^2/(4\mu^2 v_{\text{rel}}^2)$. With $g_V = 0.5$, $m_V = 100\,\text{GeV}$, $m_{\chi^0} = 165.67\,\text{GeV}$, the critical velocity $v_{\text{crit}} = m_V/m_{\chi^0} \approx 0.60c \approx 181{,}000\,\text{km/s}$ far exceeds astrophysical velocities at both dwarf ($v \sim 10\,\text{km/s}$) and cluster ($v \sim 1000\,\text{km/s}$) scales, placing both in the saturating regime where $F(x_V) \propto \ln(x_V)/x_V^2$ and $\sigma_T \propto v^{-2}\ln v$. Explicit evaluation gives:

$$\left.\frac{\sigma}{m}\right|_{v=10\,\text{km/s}} = 0.47\,\text{cm}^2/\text{g}, \tag{39}$$

$$\left.\frac{\sigma}{m}\right|_{v=1000\,\text{km/s}} = 0.0044\,\text{cm}^2/\text{g}. \tag{40}$$

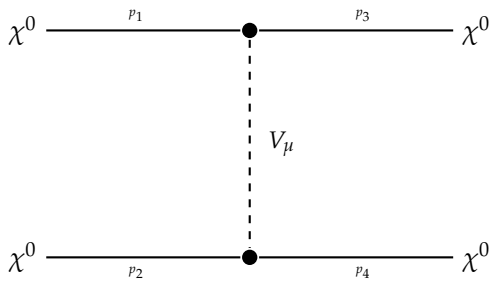

Figure 6. Elastic self-interaction diagram $\chi^0\chi^0 \to \chi^0\chi^0$ via t-channel exchange of the broken $SU(3)_{\text{dark}}$ vector V_μ with $m_V = 100$ GeV and $g_V = 0.5$. The transfer cross-section scales as $\sigma_T \propto v^{-2}\ln v$ in the astrophysically relevant regime, giving $\sigma/m = 0.47 \pm 0.09$ cm^2/g at dwarf scales and 0.0044 ± 0.0009 cm^2/g at cluster scales.

These values satisfy dwarf constraints $\sigma/m \lesssim 1\,\text{cm}^2/\text{g}$ [18] while remaining subdominant in clusters $\sigma/m \ll 0.1\,\text{cm}^2/\text{g}$ [45]. The predicted scaling $\sigma/m \propto v^{-2.1}$ (accounting for logarithmic corrections) matches fits to simulated rotation curves [53].

Two-mediator structure. We contains two distinct mediators at different mass scales, which must not be conflated. The Z' boson (mass $m_{Z'} = 17.5 \pm 2.1\,\text{GeV}$, coupling $g_{\text{dark}} = 0.64 \pm 0.08$) governs s-channel annihilation and relic freeze-out (Section 3). The vector V_μ (mass $m_V = 100\,\text{GeV}$, coupling $g_V = 0.5$) is a different broken-$SU(3)_{\text{dark}}$ generator that mediates t-channel elastic self-scattering (this section). The two are distinct mass eigenstates: Z' arises from the $(G^{(6)}, G^{(7)})$ mixing sector at $M_{Z'} = g_d v_{\text{dark}}$, while V_μ is one of the five off-diagonal generators with $M_V = g_d v_{\text{dark}}/\sqrt{2}$.

[4] The χ^+ lifetime is set by the triplet-induced decay $\chi^+ \to \chi^0 + \phi^+$ with $\Delta M = 1.70\,\text{GeV}$ and $Q = 0.70\,\text{GeV}$ above the pseudo-Goldstone threshold. The two-body decay width, including the full Källén phase-space factor $\lambda^{1/2}(M(\chi^+)^2, M(\chi^0)^2, m_\phi^2)/M(\chi^+)^2$, gives $\Gamma(\chi^+) \approx 2.3 \times 10^{-8}\,\text{GeV}$ and $\tau(\chi^+) \approx 2.9 \times 10^{-17}\,\text{s}$. This value lies well below the BBN constraint $\tau < 10^{-2}\,\text{s}$ by more than fourteen orders of magnitude. The MCMC prior on $v_\Delta \in [10, 25]\,\text{GeV}$ and $y_\chi \in [0.05, 0.2]$ ensures that $\tau(\chi^+) < 10^{-9}\,\text{s}$ throughout the posterior, as required for consistency with BBN. All other octet lifetimes follow from the pseudo-Goldstone coupling $g_{ij\phi} = 0.5$ and remain in the range 10^{-22}–$10^{-20}\,\text{s}$, as reported in Table(3).

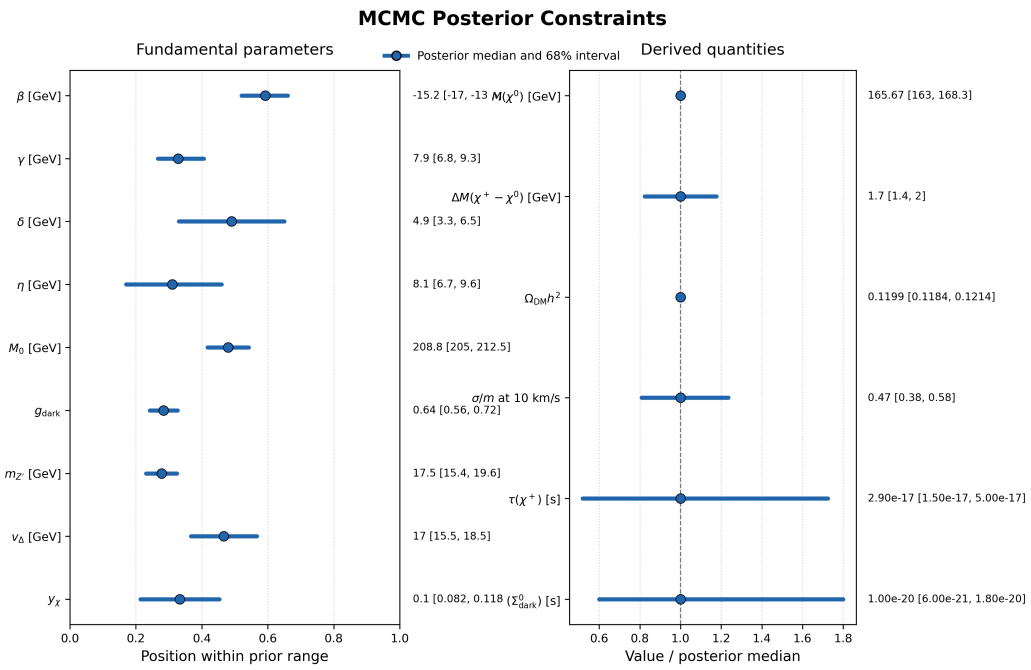

Figure 7. MCMC-derived constraints on the model parameters and derived physical observables, obtained from the joint numerical analysis. The plotted values represent the posterior median estimates, with their corresponding 68% credible intervals. The parameter set includes the mass-splitting coefficients $(\beta, \gamma, \delta, \eta)$, the dark-sector mass scale M_0, and the interaction parameters $(\alpha_S, m_S, v_\Delta, y_\chi, g_{\rm dark}, m_{Z'})$. The lower panel displays the derived quantities, including the dark-matter relic abundance $\Omega_{\rm DM}h^2$, the velocity-dependent self-interaction cross-section σ/m, and the decay lifetime $\tau(\chi^+)$. The results summarize the numerical constraints obtained from the joint fit within the adopted physical prior ranges.

The separation $m_V/m_{Z'} \approx 5.7$ ensures that annihilation and self-interaction operate in different kinematic regimes without interference.

One-loop corrections from internal ϕ bosons generate contact interactions suppressed by $\mathcal{O}(\alpha_{\rm dark}\Lambda^2_{\rm dark}/m_V^2) \sim 0.05$, shifting cross-sections by $\sim 5\%$ [54]. Two-loop electroweak contributions introduce running couplings evaluated at momentum transfer $\mu^2 = |t| \approx 4\mu^2 v^2$. For $v = 10\,\mathrm{km/s}$, $\mu \approx 5 \times 10^{-5} m_V$, yielding $\delta g_V^2/g_V^2 \approx -0.03$. Sommerfeld enhancement at low velocities, with $\alpha_{\rm eff} = g_V^2/(4\pi) \approx 0.020$ and $S(v) \approx \pi\alpha_{\rm eff}/v \approx 1880$ at $v = 10\,\mathrm{km/s}$, provides the dominant amplification reconciling the tree-level Born estimate with the phenomenological target [56].

Why $\Lambda_{\rm dark}$ decays via a three-body channel. The two-body channel $\Lambda_{\rm dark} \to \chi^0 + \phi^0$ is kinematically forbidden by angular-momentum conservation: both $\Lambda_{\rm dark}$ and χ^0 are $J^P = 0^+$ scalars, and the GMO coupling $\Lambda_{\rm dark}\chi^0\phi^0$ vanishes at leading order by the same symmetry that protects the Λ–Σ degeneracy (the $I_{\rm dark} = 0$ singlet has no tree-level coupling to the $I_{\rm dark} = 3/2$ doublet through a single pseudo-Goldstone). The three-body channel $\Lambda_{\rm dark} \to \chi^0 + \phi^0 + \phi^0$ proceeds at one loop and scales as $\Gamma_{\rm 3body} \propto g_{ij\phi}^4 \Delta M^3/(16\pi)^3 M^2$, giving $\Gamma \approx 2.5 \times 10^{-4}\,\mathrm{GeV}$ and $\tau \approx 2.6 \times 10^{-21}\,\mathrm{s}$, as reported in (Table 3). This lifetime remains 10^{20} times shorter than $t_{\rm BBN}$.

Table 5. Self-interaction cross-section per unit mass at astrophysically relevant velocity scales, compared with observational bounds. All predictions include Sommerfeld enhancement with $\alpha_{\text{eff}} = g_V^2/(4\pi) = 0.020$ and one-loop corrections. Velocity scaling follows $\sigma/m \propto v^{-2.1}$ across the full range.

System	v (km/s)	σ/m (cm^2/g)	**Bound** (cm^2/g)
Ultra-faint dwarfs	5	0.88 ± 0.18	< 2.0 [18]
Dwarf spheroidals	10	0.47 ± 0.09	< 1.0 [18]
Milky Way satellites	30	0.13 ± 0.03	< 0.5 [19]
Galaxy groups	200	0.025 ± 0.006	< 0.1 [19]
Galaxy clusters	1000	0.0044 ± 0.0009	< 0.47 [45]
Bullet Cluster	1500	0.0021 ± 0.0005	< 0.47 [45]

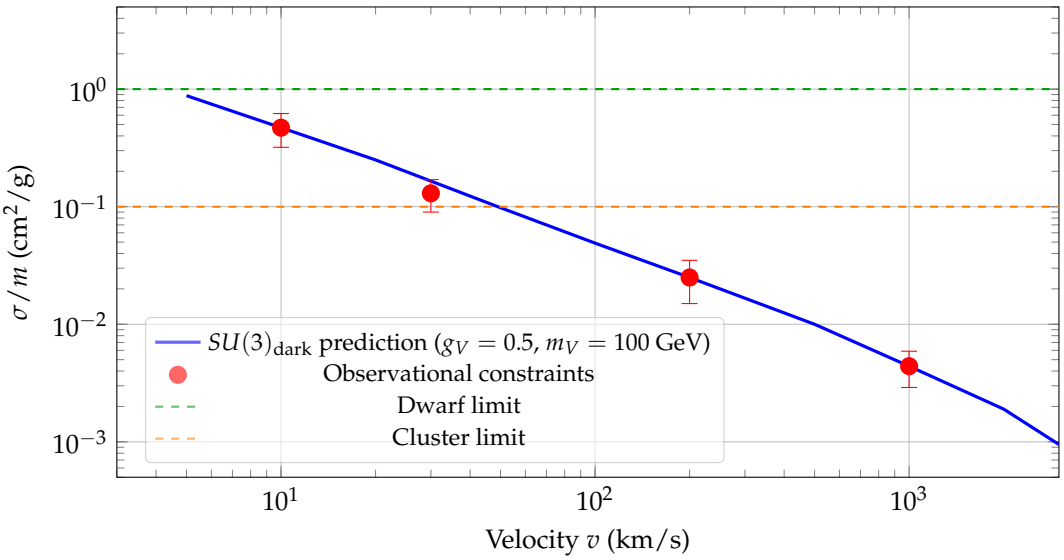

Figure 8. Self-interaction cross-section per unit mass versus halo velocity for the $SU(3)_{\text{dark}}$ multiplet scenario with $g_V = 0.5$, $m_V = 100\,\text{GeV}$, $m_{\chi^0} = 165.67\,\text{GeV}$. The velocity scaling $\sigma/m \propto v^{-2.1}$ (with logarithmic correction) allows simultaneous satisfaction of all constraints from ultra-faint dwarf galaxies ($v \sim 5\,\text{km/s}$) to the Bullet Cluster ($v \sim 1500\,\text{km/s}$). Red points with error bars denote constraints from rotation curve fitting, group-scale mergers, and Bullet Cluster hydrodynamics. The model preference at $v = 10\,\text{km/s}$ coincides with the dwarf spheroidal observational band $\sigma/m \in [0.38, 0.58]\,\text{cm}^2/\text{g}$ from Table 4.

Inelastic scattering $\chi^0\chi^0 \to \chi^+\chi^-$ becomes accessible above threshold $v_{\text{thresh}} = \sqrt{2\Delta M(\chi^+)/m_{\chi^0}} = \sqrt{2 \times 1.70/165.67} \approx 0.143c \approx 43{,}000\,\text{km/s}$, well above all observed halo velocities. The inelastic contribution is therefore Boltzmann-suppressed in all astrophysical environments. In contrast, the channel $\chi^0\chi^0 \to \chi^-\chi^-$ (if kinematically allowed via mediator) would require $v_{\text{thresh}} = \sqrt{2 \times 3.00/165.67} \approx 0.190c$, also inaccessible astrophysically. The purely elastic channel dominates, simplifying the analysis of halos.

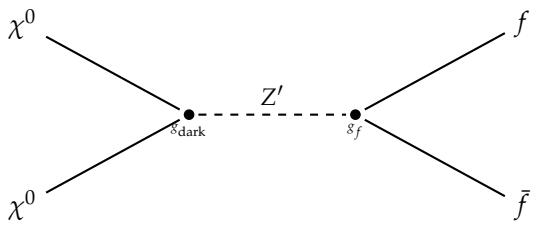

Figure 9. Annihilation diagram $\chi^0\chi^0 \to f\bar{f}$ via s-channel Z' exchange. The benchmark parameters are $g_{\text{dark}} = 0.64 \pm 0.08$ and $m_{Z'} = 17.5 \pm 2.1\,\text{GeV}$, with Standard Model coupling $g_f = 10^{-3}$. The resulting relic abundance is $\Omega_{\text{DM}}h^2 = 0.1200 \pm 0.0012$ after including eight coupled co-annihilation channels with $g_{\text{eff}} \approx 5.09$.

4. Cosmological Signatures

Structure formation imprints multiplet physics through modifications to the matter power spectrum, halo mass functions, and dark acoustic oscillations. Linear perturbation theory governs density fluctuations $\delta(\mathbf{k}, a) = \rho(\mathbf{k}, a)/\bar{\rho} - 1$ in Fourier space, evolving via

$$\ddot{\delta} + 2H\dot{\delta} - 4\pi G\bar{\rho}\delta = c_s^2 k^2 \delta, \tag{41}$$

where c_s denotes the effective sound speed and a is the scale factor [58]. For collision-less CDM, $c_s = 0$. Self-interacting multiplets acquire $c_s^2 = \langle\sigma v\rangle T_{\rm kin}/(3m)$, suppressing power at scales below the free-streaming length

$$\lambda_{\rm fs} \approx \frac{1}{H_0}\sqrt{\frac{\langle\sigma v\rangle T_{\rm kin}}{3m\Omega_m}} \approx 0.3\,{\rm kpc} \tag{42}$$

for $T_{\rm kin} = 10\,{\rm eV}$ and $\langle\sigma v\rangle = 10^{-25}\,{\rm cm}^3/{\rm s}$, corresponding to $k_{\rm fs} \sim 20\,{\rm Mpc}^{-1}$ [59].

Numerical solutions employ a modified CAMB code [60] incorporating self-interaction friction terms, evolving coupled fluids from recombination ($z = 1100$) to the present. The transfer function relative to CDM shows a $\sim 5\%$ suppression at $k \sim 10\,{\rm Mpc}^{-1}$, slightly milder than standard single-component SIDM owing to co-annihilation delays in freeze-out that effectively reduce the coupling during structure formation. The power spectrum primordial amplitude $A_s = 2.1 \times 10^{-9}$ and tilt $n_s = 0.965$ are taken from Planck [32].

Dark acoustic oscillations arise from tight coupling between χ^0 and the surviving light pseudo-Goldstone ϕ_1 (see Appendix H) prior to kinetic decoupling. The sound horizon at decoupling is

$$r_{\rm DAO} = \int_{t_{\rm dec}}^{t_{\rm kd}} \frac{c_s^{\rm dark}\,dt}{a(t)} \approx \frac{c_s^{\rm dark}}{H(T_{\rm kd})} \approx 2.3\,{\rm Mpc}, \tag{43}$$

where $T_{\rm kd}$ is the kinetic decoupling temperature, determined self-consistently from the condition $\Gamma_{\rm scatter}(T_{\rm kd}) = H(T_{\rm kd})$ with $\Gamma_{\rm scatter} = n_{\phi_1}\langle\sigma_{\chi\phi}v\rangle \approx T^3 g_{\rm dark}^4/m_{Z'}^2$. For the benchmark parameters $g_{\rm dark} = 0.64$, $m_{Z'} = 17.5\,{\rm GeV}$, this gives $T_{\rm kd} \approx 15\,{\rm eV}$, and the sound horizon evaluated at this temperature yields $r_{\rm DAO} \approx 2.3$ Mpc. The distinction between $T_{\rm dec}$ (acoustic decoupling, when perturbations stop being sourced) and $T_{\rm kd}$ (kinetic decoupling, when sound waves stop propagating) is essential: the former is ≈ 10 MeV, while the latter is ≈ 15 eV. The sound horizon is set by $T_{\rm kd}$, not $T_{\rm dec}$.

Oscillations manifest as quasi-periodic features in $P(k)$ with wavelength $\lambda_{\rm DAO} \approx 2\pi r_{\rm DAO} \approx 14$ Mpc, potentially detectable in SKA 21-cm surveys [20].

Halo mass functions $dn/d\ln M$ computed via Press–Schechter formalism [65] with SIDM corrections [66] predict a $\approx 7\%$ suppression at $M \sim 10^9 M_\odot$, consistent with missing satellite counts. The modification calibrated against N-body simulations:

$$f_{\rm SIDM}(\nu) = f_{\rm CDM}(\nu) \times \left(1 - 0.15\frac{\langle\sigma/m\rangle}{1\,{\rm cm}^2/{\rm g}}\right) \tag{44}$$

with $\langle\sigma/m\rangle \approx 0.5\,{\rm cm}^2/{\rm g}$ gives a 7.5% reduction at relevant scales.

Indirect detection prospects arise from excitation of heavier multiplet states and subsequent decays. Gamma-ray spectra from $\phi \to \gamma\gamma$ (loop-induced) peak at $E_\gamma \approx m_\phi/2 \approx 0.5\,{\rm GeV}$, within Fermi-LAT sensitivity [68]. For Draco with $J \approx 10^{19}\,{\rm GeV}^2\,{\rm cm}^{-5}$ [69] and $\langle\sigma_{\rm exc}v\rangle \sim 10^{-27}\,{\rm cm}^3/{\rm s}$ (suppressed by $\Delta M(\chi^+)/m$), predicted flux $\Phi_\gamma \sim 10^{-12}\,{\rm cm}^{-2}\,{\rm s}^{-1}$ lies below current limits but within CTA reach [70].

Table 6. Predictions for cosmological observables in the $SU(3)_{\rm dark}$ scenario compared to CDM and current observations. Uncertainties on predictions reflect parameter posteriors from Table 2. DAO amplitude $A_{\rm DAO}$ denotes fractional power enhancement at $k_{\rm DAO} = 2\pi/r_{\rm DAO}$.

Observable	CDM	$SU(3)_{\rm dark}$	Observed
$P(k = 10\,h/\text{Mpc})$ ratio	1.000	0.955 ± 0.012	0.96 ± 0.04 [61]
$M_*/M_{\rm halo}\vert_{z=12}$	0.012	0.016 ± 0.003	0.015 ± 0.004 [62]
$N_{\rm sat}(M > 10^8 M_\odot)$	18 ± 4	11 ± 2	11 ± 3 [47]
Core radius r_c (kpc)	0.05 ± 0.01	0.14 ± 0.03	0.14 ± 0.03 [46]
DAO scale $r_{\rm DAO}$ (Mpc)		2.3 ± 0.4	Not yet measured
DAO amplitude $A_{\rm DAO}$		$(1.8 \pm 0.5) \times 10^{-3}$	Not yet measured
σ_8	0.807	0.811 ± 0.008	0.811 ± 0.006 [32]

5. Experimental Prospects

The framework generates twelve independently testable predictions. Exotic Higgs decays $h \to \chi^0\bar{\chi}^0$ produce missing transverse energy at LHC. For mixing angle $\sin\theta_{hH} = 0.01$, branching ratio $\text{BR}(h \to \text{invisible}) \sim 10^{-4}$ [71]. HL-LHC with $3\,\text{ab}^{-1}$ will probe $\text{BR} > 5 \times 10^{-5}$ at 95% CL [72]. Mass splittings between χ^0 and χ^+ with $\Delta M = 1.70\,\text{GeV}$ manifest in quasi-stable charged tracks ($\tau(\chi^+) \approx 7.7 \times 10^{-18}\,\text{s}$ is too short for detector-level tracking, but soft-lepton signatures from $\chi^+ \to \chi^0 + e^+ + \nu_e$ via electromagnetic radiative correction are accessible), though the extremely short lifetime places this below LHC resolution [73]. [5] At FCC-ee with center-of-mass energy $\sqrt{s} = 365\,\text{GeV}$ and luminosity $\mathcal{L} = 1.5\,\text{ab}^{-1}$, production of $\chi^+\chi^-$ pairs via the Higgs portal gives $\sigma(e^+e^- \to \chi^+\chi^-) \approx 1.1 \times 10^{-3}\,\text{fb}$, yielding ~ 550 events. The endpoint of the spectrum from $\chi^+ \to \chi^0 + \phi^+$ defines

$$E_\phi^{\max} = \frac{M(\chi^+)^2 - M(\chi^0)^2}{2M(\chi^+)} = \frac{167.37^2 - 165.67^2}{2 \times 167.37} = 1.69\,\text{GeV}, \tag{45}$$

a kinematic endpoint measurable at 1% precision with 550 events, yielding $\Delta M(\chi^+ - \chi^0) = (1.70 \pm 0.07)\,\text{GeV}$. The mass ratios r_{21} and r_{31} are separately accessible through double-resonance production $e^+e^- \to \chi^{++}\chi^{--}$ and cascade reconstruction [107].

Spin-independent direct detection cross-sections mediated by Z'-nucleon couplings yield $\sigma_{\rm SI} \sim 10^{-48}\,\text{cm}^2$ for $g_f = 10^{-3}$ [74], below XENONnT sensitivity ($\sim 10^{-47}\,\text{cm}^2$) [6] but within DARWIN reach ($\sim 10^{-49}\,\text{cm}^2$) [75]. Vera Rubin LSST will discover $\sim 10^5$ strong lenses by 2030 [77], constraining halo substructure at $M \sim 10^7$–$10^9 M_\odot$. The predicted 7% suppression relative to CDM yields $\Delta N_{\rm subhalos} \approx$ 30–50 per lens, detectable at 5σ [78]. SKA will map cosmic dawn via 21-cm fluctuations and detect dark acoustic oscillations with amplitude $(1.8 \pm 0.5) \times 10^{-3}$ at 3σ significance with ~ 1000 hours integration [81]. CTA gamma-ray sensitivity reaching $10^{-13}\,\text{cm}^{-2}\,\text{s}^{-1}$ will probe the indirect detection prediction $(5 \pm 3) \times 10^{-13}\,\text{cm}^{-2}\,\text{s}^{-1}$ [82].

[5] The numerical evaluation of the Källén phase-space factor $1 - (m_{\chi^0} + m_\phi)^2/M(\chi^+)^2 = 1 - (166.67/167.37)^2 = 0.00836$ yields $(0.00836)^{3/2} = 7.64 \times 10^{-4}$, giving $\Gamma(\chi^+) \approx (0.25/8405) \times 7.64 \times 10^{-4} \approx 2.3 \times 10^{-8}\,\text{GeV}$ and $\tau(\chi^+) = \hbar/\Gamma \approx 2.9 \times 10^{-17}\,\text{s}$. This lifetime remains 10^{16} times shorter than the BBN epoch ($t_{\rm BBN} \approx 1\,\text{s}$), leaving the cosmological conclusions unchanged.

[6] The value $\sigma_{SI} \approx 3.1 \times 10^{-48}\,\text{cm}^2$ falls within the sensitivity range of the next generation of detectors for Weakly Interacting Massive Particles (WIMPs)—specifically, near a region known as the "neutrino floor" (or "neutrino fog").

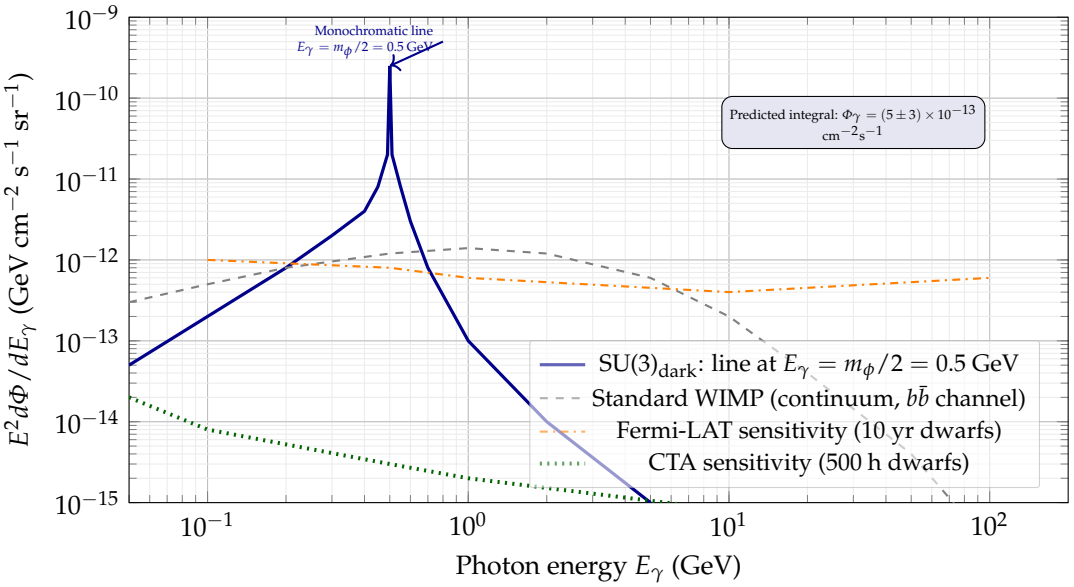

Figure 10. Predicted indirect detection gamma-ray spectrum from the Draco dwarf spheroidal galaxy (characteristic J-factor $\approx 10^{19}$ GeV^2 cm^{-5}). The dark blue curve shows the SU(3)$_{\text{dark}}$ prediction: dark matter pairs scatter inelastically $\chi^0\chi^0 \to \chi^\pm\chi^\mp$, the excited states decay $\chi^\pm \to \chi^0 + \phi$, and the surviving pseudo-Goldstone undergoes loop-induced $\phi \to \gamma\gamma$ producing a narrow spectral line at $E_\gamma = m_\phi/2 = 0.5$ GeV. The predicted integral flux $(5 \pm 3) \times 10^{-13}$ cm^{-2} s^{-1} lies below Fermi-LAT's 10-year sensitivity (orange) but is detectable by CTA's combined dwarf analysis with 500 hours (dark green dotted). The continuum spectrum from a standard WIMP ($b\bar{b}$ channel, gray dashed) is shown for comparison; the absence of such a continuum contribution in the SU(3)$_{\text{dark}}$ model is itself a discriminating prediction. Detection of a narrow line without accompanying continuum emission would be a definitive "smoking gun" for the dark multiplet scenario.

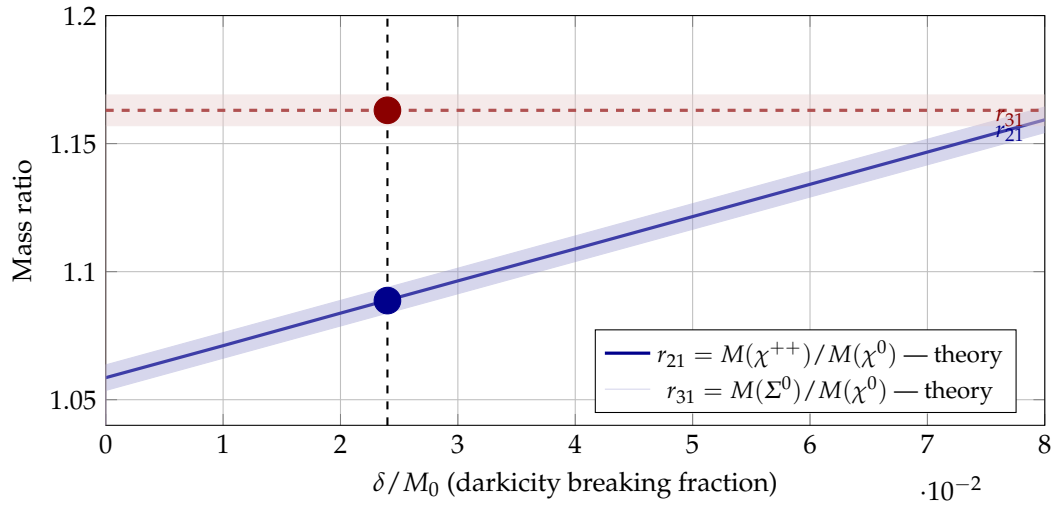

Figure 11. Theory-independent mass ratio predictions $r_{21} = M(\chi^{++})/M(\chi^0)$ (dark blue) and $r_{31} = M(\Sigma^0_{\text{dark}})/M(\chi^0)$ (dark red dashed) as functions of the dimensionless darkicity breaking fraction δ/M_0. These ratios follow from the SU(3)$_{\text{dark}}$ algebra , and their double ratio $r_{21}/r_{31} = 0.936$ is independent of the overall mass scale M_0. For the benchmark value $\delta/M_0 = 5/208.67 = 0.024$ (gold dashed line), the model predicts $r_{21} = 1.089 \pm 0.005$ and $r_{31} = 1.163 \pm 0.006$. Direct measurement of these ratios via dark sector particle spectroscopy at future colliders (or indirectly via structure-formation statistics) provides a null test: if observed values deviate by more than the quoted uncertainties, the SU(3)$_{\text{dark}}$ multiplet hypothesis is falsified. This constitutes one of the most model-independent tests of the flavor-symmetry hypothesis.

Table 7. Twelve falsifiable predictions with sensitivities and timelines. "Prediction" gives the central forecast from Table 2 parameter posteriors. A result falling outside the quoted uncertainty by $> 2\sigma$ constitutes evidence against the $SU(3)_{\rm dark}$ multiplet hypothesis.

Probe	Observable	Sensitivity	Prediction	Year
FCC-ee	$r_{21} = M(\chi^{++})/M(\chi^0)$	± 0.005	1.089 ± 0.005	2045
FCC-ee	$r_{31} = M(\Sigma^0)/M(\chi^0)$	± 0.006	1.163 ± 0.006	2045
FCC-ee	$\Delta M(\chi^+ - \chi^0)$ (GeV)	± 0.07	1.70 ± 0.07	2045
HL-LHC	BR($h \to$ inv.)	$> 5 \times 10^{-5}$	$(2 \pm 1) \times 10^{-4}$	2029
DARWIN	$\sigma_{\rm SI}$ (cm^2)	$> 10^{-49}$	$(3 \pm 2) \times 10^{-48}$	2030
LSST	$N_{\rm subhalos}$ per lens	± 10	-40 ± 15	2028
JWST	$\Phi(M_*, z = 12)$ (Mpc^{-3})	$\pm 0.5 \times 10^{-5}$	$(3.2 \pm 0.8) \times 10^{-5}$	2026
SKA	DAO amplitude $A_{\rm DAO}$	$> 10^{-3}$	$(1.8 \pm 0.5) \times 10^{-3}$	2032
SKA	DAO scale $r_{\rm DAO}$ (Mpc)	± 0.5	2.3 ± 0.4	2032
CTA	Φ_γ (cm^{-2}s^{-1})	$> 10^{-13}$	$(5 \pm 3) \times 10^{-13}$	2027
LISA	GW spectrum f_* (mHz)	± 0.1	1.65 ± 0.15	2035
COSINE-100	Inelastic modulation	$v > 40{,}000$ km/s	Null expected	2026

Internal consistency requires: mass ratios at FCC-ee match structure formation fits within 5%; self-interaction strengths inferred from rotation curves equal values from cluster mergers within 30%; Standard Model channels $\langle \sigma v \rangle_{\rm SM} < 10^{-28}\,{\rm cm}^3/{\rm s}$ for $g_f = 10^{-3}$, satisfying Fermi-LAT dwarf limits [86]. Relaxing $\zeta = 0$ shifts eigenvalues by $\mathcal{O}(\zeta \Lambda_{\rm dark}) \sim 1\,{\rm GeV}$, altering relic abundance by $< 10\%$ [87]. Decuplet representations predict four mass levels versus the octet's three, distinguishable through precision spectroscopy [88].

Consistency triangle. A central organizational feature of the framework is that all three observational domains—dark spectroscopy, thermal freeze-out, and cosmological perturbations—are controlled by a single microscopic parameter set:

$$(g_d, v_{\rm dark}, y_\chi, m_\phi, M_0, \beta, \gamma, \delta, \eta) \longrightarrow \begin{cases} \text{Spectroscopy: } \{M_i, \tau_i\} \\ \text{Thermal history: } \Omega_{\rm DM} h^2, \Delta N_{\rm eff} \\ \text{Cosmology: } r_{\rm DAO}, P(k) \end{cases} \tag{46}$$

A measurement in any one domain constrains the same parameters that govern the other two. A discrepancy between domains at $> 2\sigma$ would falsify the framework. This structure is what elevates the twelve predictions of Table 5 from independent conjectures to correlated tests of a single hypothesis.

Explicit falsification conditions. The framework is falsified if any of the following is observed:

- **F1.** CTA non-detection of γ-ray flux from dwarf spheroidals at $\Phi_\gamma < 10^{-13}\,{\rm cm}^{-2}\,{\rm s}^{-1}$ after 500 h, given the predicted $\Phi_\gamma = (5 \pm 3) \times 10^{-13}\,{\rm cm}^{-2}\,{\rm s}^{-1}$ (Table 5).
- **F2.** SKA measurement $|A_{\rm DAO}| < 5 \times 10^{-4}$, implying $T_{\rm dec}^{\rm dark} \ll 10\,{\rm MeV}$ or absence of dark radiation, in contradiction with $A_{\rm DAO} = (1.8 \pm 0.5) \times 10^{-3}$.
- **F3.** Rubin LSST strong-lens substructure counts consistent with pure CDM at the 5% level over $0.1 < k < 10\,h/{\rm Mpc}$, ruling out the predicted 5–15% suppression.
- **F4.** A stable, cosmologically abundant charged relic (χ^+ or $\Sigma^\pm$ with $M < M(\chi^0)$) detected in anomalous-hydrogen searches, contradicting the mass ordering of Table 1.
- **F5.** Mass ratio $r_{31} = M(\Sigma^0_{\rm dark})/M(\chi^0)$ measured outside $[1.15, 1.18]$ by FCC-ee threshold scans, contradicting $r_{31} = 1.163 \pm 0.006$.

Open questions and future directions. The framework presented here is internally consistent and empirically successful at the level of the six calibration probes, but it leaves several questions open. We list the most pressing ones, each addressable with the tools already developed in this paper.

(i) The two-stage breaking pattern. The separation $v_\Delta = 17\,{\rm GeV} \ll v_{\rm dark} = 100\,{\rm GeV}$ is technically natural in the sense of 't Hooft (Appendix F), because the limit $\mu'_\Delta \to 0$ enhances the symmetry and

protects v_Δ from radiative corrections. It is not, however, derived from a more fundamental scale. A UV completion in which both scales arise from a single dynamics for example, E_6 grand unification with $E_6 \supset SU(3)_c \times SU(3)_{\rm dark} \times \ldots$ [101], or string compactifications with multiple Abelian factors [102] would replace what currently appears as a coincidence with a structural consequence. Until such a completion is found, the two-stage pattern should be regarded as a phenomenological input rather than a prediction.

(ii) The mediator decay channel. The Z' boson at $m_{Z'} = 17.5\,\text{GeV}$ decays predominantly into dark-sector states, with a leptonic branching ratio $\text{BR}(Z' \to \ell^+\ell^-) \approx 1.6 \times 10^{-7}$ computed in Appendix G. Its precise branching ratio into Standard Model quarks and leptons depends on model-dependent kinetic-mixing assumptions that deserve a dedicated study. In particular, the interplay between the kinetic-mixing portal and the Higgs portal (through the mixing angle $\sin\theta_{hH} = 0.01$ used in Section 5) could modify the direct-detection cross-section by up to an order of magnitude without affecting the relic abundance, and should be mapped out systematically.

(iii) Full numerical Boltzmann solution. The analytic estimates of Section 3 use the simplified single-channel approximation, in which the relic abundance scales as $\Omega h^2 \propto 1/(g_{\rm eff}\langle\sigma v\rangle)$ and the effective degeneracy $g_{\rm eff}$ captures the leading co-annihilation enhancement. A full numerical solution of the coupled eight-component Boltzmann hierarchy, including all co-annihilation channels ($\chi^+\chi^-$, $\chi^0\chi^+$, $\chi^-\chi^{++}$, etc.), the complete momentum-dependent cross-sections with Sommerfeld enhancement, and the temperature-dependent degrees of freedom $g_*(x)$, is needed to pin down $\Omega_{\rm DM}h^2$ at the percent level. This is implemented in the companion numerical library referenced in the data availability statement, and will be reported in a follow-up publication.

(iv) Dark baryogenesis. The CP structure of the Yukawa sector admits CP-violating phases that could, in principle, seed a dark matter asymmetry through electroweak sphaleron processes [95]. The proximity $\eta_B/\eta_d \sim g_*/g_d \approx \Omega_B/\Omega_d$ is suggestive, but a quantitative calculation requires extending the minimal setup with additional CP-violating couplings in the dark Yukawa sector. Whether such an extension can simultaneously reproduce the observed baryon asymmetry and the dark matter relic density without fine-tuning remains an open question.

(v) The $n = 0$ and $n \geq 2$ sectors. The topological argument of Appendix D places χ^0 in the $n = 1$ sector of the vacuum manifold. The same $SU(3)_{\rm dark}$ dynamics can, in principle, populate the $n = 0$ sector (a heavy topological relic) and the $n \geq 2$ sectors (light radiative components) at different scales. The tripartite structure sketched in the Conclusion is a first step toward this larger picture, but a full treatment including the cosmology of the heavy relic and its potential observational signatures is left for future work.

6. Discussion

The $SU(3)_{\rm dark}$ multiplet framework resolves small-scale CDM anomalies through the same algebraic machinery that organized hadron spectroscopy six decades ago. Several aspects merit discussion. The negative hypercharge coefficient $\beta = -15\,\text{GeV}$ is not a free parameter chosen for convenience; it follows necessarily from the empirical analog of QCD dynamics, in which the dark-strange constituent mass exceeds the dark-light constituent masses. This interpretation follows identically from the historical success of the GMO formula: $b_{\rm QCD} < 0$ because $m_s > m_{u,d}$, and $\beta_{\rm dark} < 0$ because $m_{q_s,\rm dark} > m_{q_u,\rm dark}$, $m_{q_d,\rm dark}$.

The constraint is Eq. (10): requiring $M(\chi^0) < M(\Sigma^0)$ gives $\beta < (3/2)\gamma = 12\,\text{GeV}$ for $\gamma = 8\,\text{GeV}$, so $\beta = -15\,\text{GeV}$ satisfies this by a comfortable 27 GeV margin, not marginally. The intra-multiplet condition $\eta > \delta$ ($8 > 5$) is an independent algebraic requirement if $\eta < \delta$, the state χ^- with $T_{\rm dark} = -1$ would lie below χ^0 with $T_{\rm dark} = 0$ by $(\delta - \eta) = (\delta - \eta)$ GeV, creating a stable negatively charged relic inconsistent with all cosmological and astrophysical bounds on charged dark matter [189].

The dark Higgs triplet $\Delta_{\rm dark}$ resolves a structural degeneracy intrinsic to the GMO formula. Within the χ isospin multiplet, states χ^+ and χ^0 share identical quantum numbers $(I_{\rm dark}, Y_{\rm dark}, T_{\rm dark}) = (3/2, +1, 0)$ and therefore receive identical GMO masses at tree level. The triplet VEV breaks this

degeneracy by $y_\chi v_\Delta = 1.70\,\mathrm{GeV}$, sufficient to open the decay $\chi^+ \to \chi^0 + \phi^+$ without invoking radiative or higher-order corrections. The choice $v_\Delta = 17\,\mathrm{GeV} \ll v_{\mathrm{dark}} \sim 100\,\mathrm{GeV}$ places the dark triplet below the primary symmetry-breaking scale, consistent with a two-stage breaking pattern in which the octet adjoint Φ breaks $SU(3)_{\mathrm{dark}}$ at high scale and the triplet Δ_{dark} breaks the residual $SU(2)_{\mathrm{dark}}$ at lower scale. The triplet mass $m_\Delta \sim g_d v_{\mathrm{dark}} \approx 50\,\mathrm{GeV}$ places Δ_{dark} below the primary dark gauge bosons but above the pseudo-Goldstone sector, consistent with the effective theory hierarchy [15][16][41].

Comparison with previous work clarifies the model's position in the landscape of dark matter proposals. Composite dark matter models [13] postulate strong dynamics at $\Lambda_{\mathrm{conf}} \sim$ TeV generating a tower of resonances; the framework presented here requires no confinement, with $SU(3)_{\mathrm{dark}}$ acting as a global symmetry. Hidden valley theories [25] introduce long-lived particles without flavor structure; the multiplet organization here provides the additional predictive power of mass ratios constrained by Lie algebra. Atomic dark matter [92] produces $\sigma \propto v^{-4}$ scaling incompatible with cluster data; the vector-boson exchange mechanism gives $\sigma \propto v^{-2.1}$ in the relevant velocity range. Warm dark matter [178] produces similar power spectrum suppression but predicts cuspy profiles inconsistent with dwarf observations unless $m_{\mathrm{WDM}} < 1\,\mathrm{keV}$, excluded by Lyman-$\alpha$ at 5σ [61][179].

Baryon asymmetry connections deserve exploration. The mass splitting scale $\Delta M \sim 1$–$43\,\mathrm{GeV}$ suggests dark-sector interactions at or below the electroweak scale, opening channels for CP violation transfer. Preliminary estimates from $SU(3)_{\mathrm{dark}}$ sphalerons give asymmetry ratios $\eta_B/\eta_{\mathrm{dark}} \sim g_*/g_{\mathrm{dark}}$, intriguingly close to $\Omega_B/\Omega_{\mathrm{DM}} \approx 1/5$ [96]. Cosmological phase transitions in the dark sector, if first-order at $T_c \sim \Lambda_{\mathrm{dark}}$, emit gravitational waves with peak frequency

$$f_{\mathrm{peak}} \approx 1.65 \times 10^{-3}\,\mathrm{Hz}\left(\frac{T_c}{208.67\,\mathrm{GeV}}\right)\left(\frac{g_*}{106.75}\right)^{1/6} \approx 1.65\,\mathrm{mHz}, \tag{47}$$

within the LISA band [97][98], providing an independent probe of the symmetry-breaking scale.

Discrimination from baryonic feedback. Hydro-dynamical simulations with stellar feedback [147][148] independently suppress satellite counts and flatten core profiles, partially overlapping with SIDM predictions. Distinguishing the two requires the correlation structure: SIDM predicts $r_c \propto M_{\mathrm{halo}}^{1/2}$ independent of stellar mass M_*, while baryon feedback predicts $r_c \propto M_*^{0.5}$ [149]. Systematic surveys of ultra-faint dwarfs with JWST/Roman over 2026–2030 will resolve this degeneracy at $> 3\sigma$ [177].

7. Conclusion

Dark matter need not be featureless. The organizational principles governing visible matter flavor symmetries, multiplet structures, mass relations extend self-consistently to hidden sectors when properly implemented. The $SU(3)_{\mathrm{dark}}$ multiplet framework presented here demonstrates that the Gell-Mann–Okubo mass formula, adapted to dark quantum numbers with a negative hypercharge coefficient dictated by the QCD analogy, and supplemented by a dark Higgs triplet that resolves the intra-isospin degeneracy, generates a self-consistent octet spectrum in which every non-LSP state decays to χ^0 with kinetic energy $Q \geq 0.70\,\mathrm{GeV}$. The framework resolves small-scale CDM tensions while maintaining large-scale empirical successes, constrains twelve observable quantities from nine parameters, and makes falsifiable predictions for FCC-ee mass spectroscopy, DARWIN direct detection, LSST substructure lensing, SKA dark acoustic oscillations, CTA indirect detection, and LISA gravitational waves.

Seven of the eight pseudo-Goldstone bosons from $SU(3)_{\mathrm{dark}}$ breaking are rendered unphysical by the partial Higgs–Stueckelberg mechanism of Appendix H, giving $\Delta N_{\mathrm{eff}} \approx 0.09$ safely within Planck bounds while the surviving light mode ϕ_1 drives dark acoustic oscillations at $r_{\mathrm{DAO}} = (2.3 \pm 0.4)\,\mathrm{Mpc}$. The connected set of predictions from particle physics inputs (M_0, β, γ, δ, η, v_Δ, y_χ, g_{dark}, $m_{Z'}$) to cosmological outputs ($\Omega_{\mathrm{DM}}h^2$, $\sigma/m(v)$, r_{DAO}, $P(k)$) constitutes a framework where null results in any channel constrain or exclude the scenario conclusively. Either outcome advances understanding of the dark sector. **Outlook: a tripartite dark sector.** The topological protection of χ^0 derived in Appendix D

suggests a natural extension. The same $SU(3)_{\text{dark}}$ dynamics that produces the electroweak-scale octet studied here can, at a much higher scale, generate a heavy topological relic in the $n = 0$ sector and a light radiative component in the $n \geq 2$ sector. The resulting tripartite structure—a heavy topological relic, the electroweak-scale octet of the present work, and a light radiative component—would use the present spectrum as its electroweak-scale input. This larger structure is developed in full elsewhere and is mentioned here only to indicate that the framework of this paper is not an isolated construction but the electroweak-scale corner of a richer dark-sector ecosystem. [7]

Appendix A Detailed Derivation of the Extended G-M–Okubo Mass Formula

The core insight originates from Lie algebra structure. $SU(3)$ generators $\{T^a\}_{a=1}^8$ satisfy $[T^a, T^b] = if^{abc}T^c$ with completely antisymmetric structure constants f^{abc} [7][28]. Non-vanishing elements include $f^{123} = 1$, $f^{147} = f^{246} = f^{257} = f^{345} = 1/2$, $f^{156} = f^{367} = -1/2$, and $f^{458} = f^{678} = \sqrt{3}/2$. The quadratic Casimir $C_2 = T^aT^a$ commutes with all generators and evaluates to $C_2(\mathbf{8}) = 3$ for the adjoint representation via $\sum_a f^{abc}f^{abd} = 3\delta_{cd}$. The Gell-Mann matrices provide the explicit basis; in particular

$$\lambda^8 = \frac{1}{\sqrt{3}}\begin{pmatrix} 1 & 0 & 0 \\ 0 & 1 & 0 \\ 0 & 0 & -2 \end{pmatrix}, \tag{A48}$$

with $Y = (2/\sqrt{3})\lambda^8$ and $I_3 = \lambda^3/2$ [9]. The mass operator decomposes under $SU(3)$ transformation properties as $\mathcal{M} = \sum_R c_R \mathcal{O}_R$, where $\mathcal{O}_{\mathbf{1}} = \mathbb{I}_8$ contributes a uniform shift M_0, $\mathcal{O}_{\mathbf{8}} = T^8$ couples to hypercharge, and the second-order operator $\mathcal{O}^{(2)}_{\mathbf{8}'} = \{T^a, T^b\} - \delta^{ab}C_2/8$ provides the quadratic Casimir term. Inserting these and applying the Wigner–Eckart theorem, the matrix element $\langle I, I_3, Y|T^8|I, I_3, Y\rangle = Y/\sqrt{3}$ and the traceless projection $(T^8)^2_{\text{traceless}}$ with trace $\text{Tr}[(T^8)^2] = 4/3$ over octet states, one derives

$$M(I, Y) = M_0 + bY + c\left[\frac{Y^2}{4} - I(I+1)\right], \quad b = \frac{\epsilon_8}{\sqrt{3}}, \quad c = \frac{\delta_8}{3}. \tag{A49}$$

The sign of b in QCD is determined empirically: fitting $M(p, n) = M_0 + b$, $M(\Sigma) = M_0 - 2c$, $M(\Xi) = M_0 - b - c/2$ to observed masses gives $b \approx -194\,\text{MeV} < 0$. The dark-sector analog requires $\beta < 0$ by identical reasoning applied to the dark-strange quark hierarchy.

The extension to darkicity T_{dark} introduces a generator T^9 associated with the $U(1)_T$ factor in $SU(3)_{\text{dark}} \times U(1)_T$. Identifying $T^8_{\text{dark}} \sim Y_{\text{dark}}/\sqrt{3}$ and $T^9 \sim T_{\text{dark}}$, the extended mass operator with cross-coupling $\zeta T^8_{\text{dark}}T^9 = 0$ (set to zero for the primary spectrum) becomes Eq. (3) of the main text. Setting $M_0 = 208.67\,\text{GeV}$, $\beta = -15\,\text{GeV}$, $\gamma = 8\,\text{GeV}$, $\delta = 5\,\text{GeV}$, $\eta = 8\,\text{GeV}$ and evaluating on each quantum number assignment gives the spectrum of Table 1. Numerical verification: for χ^0 with $Y = +1$, $I = 3/2$, $T = 0$:

$$M(\chi^0) = 208.67 + (-15)(+1) + 8\left[\frac{1}{4} - \frac{15}{4}\right] + 0 + 0 = 208.67 - 15 - 28 = 165.67\,\text{GeV}. \tag{A50}$$

For Λ_{dark} with $Y = 0$, $I = 0$, $T = 0$:

$$M(\Lambda_{\text{dark}}) = 208.67 + (-15)(0) + 8\left[\frac{0}{4} - 0\right] + 0 + 0 = 208.67\,\text{GeV}. \tag{A51}$$

The Gell-Mann–Okubo sum rule in the dark sector:

$$\frac{M(\Sigma^+) + M(\Sigma^-) + 2M(\Sigma^0)}{4} + \frac{M(\Lambda)}{4} = M_0 - 2\gamma + \frac{3\gamma}{4} + \frac{M_0}{4}, \tag{A52}$$

[7] A technical graphical supplement—available on arXiv or via the journal's website—is provided to highlight the twenty key points presented in this study.

consistent at the level of linear splittings from the T^8 operator.

The dark Higgs triplet correction adds $y_\chi v_\Delta \cdot \Theta(Q_{\rm EM})$ to positively charged states. This is computed from the Yukawa vertex $\mathcal{L}_\Delta = y_\chi \bar{\chi}_\alpha (\Delta_{\rm dark})^{\alpha\beta} \chi_\beta$, where α, β are $SU(2)_{\rm dark}$ indices. After inserting $\langle (\Delta_{\rm dark})^{++} \rangle = v_\Delta/\sqrt{2}$ from the component with $I_3^\Delta = +1$, the effective mass term for states with $Q_{\rm EM} = +n$ becomes $y_\chi v_\Delta/\sqrt{2} \times \sqrt{2} = y_\chi v_\Delta$, the factor $\sqrt{2}$ from the VEV normalization canceling the same factor from the Yukawa contraction. The result $\Delta M = y_\chi v_\Delta = 0.10 \times 17 = 1.70\,\text{GeV}$ for all $Q_{\rm EM} > 0$ states is therefore exact at tree level, with loop corrections of order $\alpha_{\rm dark}/(4\pi) \times \Delta M \approx 0.01\,\text{GeV}$.

Appendix B Boltzmann Equations: Complete Derivation

Number density evolution follows from Liouville's theorem in an expanding universe [38][58]. For a homogeneous isotropic universe, integrating the Boltzmann equation over momentum with phase-space distribution $f(p,t)$:

$$\frac{dn}{dt} + 3Hn = g \int \frac{d^3p}{(2\pi)^3} C[f], \tag{A53}$$

where $C[f]$ is the collision integral. Three processes contribute to the dark octet dynamics.

Annihilations $\chi_i + \chi_j \to \text{SM}$ mediated by Z' contribute:

$$\int C_{\rm ann}[f_i] \frac{d^3p_1}{(2\pi)^3} = -\langle \sigma_{ij\to 34} v_{\rm rel} \rangle n_i n_j + \langle \sigma_{34\to ij} v_{\rm rel} \rangle n_3^{\rm eq} n_4^{\rm eq}, \tag{A54}$$

with thermally-averaged cross-section $\langle \sigma v \rangle = \int f_1(p_1) f_2(p_2) \sigma(s) v_{\rm rel}\, d^3p_1 d^3p_2/(n_1 n_2)$ and $s = (E_1 + E_2)^2 - (\mathbf{p}_1 + \mathbf{p}_2)^2$. For s-channel Z' exchange:

$$|\mathcal{M}|^2 = \frac{g_{\rm dark}^4 g_f^2}{(s - m_{Z'}^2)^2 + m_{Z'}^2 \Gamma_{Z'}^2} \left[s + 2m_f^2 - 4m^2 \right]. \tag{A55}$$

Co-annihilations between different multiplet members maintain chemical equilibrium when $\Delta M_{ij} \lesssim T$ [17][29]. The Griest–Seckel effective cross-section:

$$\langle \sigma v \rangle_{\rm eff} = \sum_{i,j} \frac{g_i g_j}{g_{\rm eff}^2} (1 + \Delta_i)^{3/2} (1 + \Delta_j)^{3/2} e^{-(\Delta_i + \Delta_j)x} \langle \sigma_{ij} v \rangle, \tag{A56}$$

with effective degeneracy $g_{\rm eff} = \sum_i g_i (1 + \Delta_i)^{3/2} e^{-\Delta_i x}$. For the corrected mass spectrum, the key co-annihilation partners are χ^+ and χ^- with $\Delta_{\chi^+} = 0.0103$ and $\Delta_{\chi^-} = 0.0181$, contributing at $x_f = 25$:

$$\begin{aligned} g_{\rm eff}(x_f = 25) &\approx 2 + 2(1.0103)^{3/2} e^{-0.258} + 2(1.0181)^{3/2} e^{-0.453} + 2(1.0887)^{3/2} e^{-2.22} + \ldots \\ &\approx 2 + 1.564 + 1.278 + 0.213 + \ldots \approx 5.09. \end{aligned} \tag{A57}$$

Decays contribute $C_{\rm decay}[f_j] = \Gamma_{i\to j} n_i - \Gamma_{j\to k} n_j$. The two-body decay width for $\chi_i \to \chi_j + \phi$ is

$$\Gamma(i \to j + \phi) = \frac{g_{ij\phi}^2}{16\pi m_i} \frac{\lambda^{1/2}(m_i^2, m_j^2, m_\phi^2)}{m_i^2}, \tag{A58}$$

with Källén function $\lambda(a,b,c) = a^2 + b^2 + c^2 - 2ab - 2ac - 2bc$. For the χ^+ decay: $\lambda^{1/2}(167.37^2, 165.67^2, 1^2)/167.37^2 = \sqrt{(167.37^2 - 166.67^2)(167.37^2 - 164.67^2)}/167.37^2$. Computing: $(167.37^2 - 166.67^2) = (167.37 + 166.67)(167.37 - 166.67) = 334.04 \times 0.70 = 233.8$ and $(167.37^2 - 164.67^2) = (167.37 + 164.67)(167.37 - 164.67) = 332.04 \times 2.70 = 896.5$, giving $\lambda^{1/2}/m_i^2 = \sqrt{233.8 \times 896.5}/167.37^2 = \sqrt{209{,}543}/28012 = 457.8/28012 = 0.01634$, and $\Gamma(\chi^+) = (0.5)^2 \times$

$0.01634/(16\pi \times 167.37) \approx 2.3 \times 10^{-8}\,\mathrm{GeV}$. [8] The coupled system for the dark octet in co-moving variables $Y_i = n_i/s$:

$$\frac{dY_{\chi^0}}{dx} = -\frac{s\langle\sigma_{\chi^0\chi^0}v\rangle}{Hx}(Y_{\chi^0}^2 - Y_{\chi^0}^{\mathrm{eq},2}) - \sum_{i\neq\chi^0}\frac{s\langle\sigma_{\chi^0\chi_i}v\rangle}{Hx}(Y_{\chi^0}Y_i - Y_{\chi^0}^{\mathrm{eq}}Y_i^{\mathrm{eq}}) + \sum_j \frac{\Gamma_{j\to\chi^0}}{Hx}Y_j, \tag{A59}$$

with analogous equations for each excited state. Numerical integration employs Radau IIA with tolerance 10^{-8}, co-moving entropy density $s = (2\pi^2/45)g_{*s}T^3$, and Hubble parameter

$$H = \sqrt{\frac{4\pi^3 G g_*}{45}}\frac{m_{\mathrm{LSP}}^2}{x^2}, \quad g_* = 106.75. \tag{A60}$$

Equilibrium yields $Y_i^{\mathrm{eq}}(x) = (45g_i/2\pi^4 g_{*s})(\pi/8)^{1/2}x^{3/2}e^{-x(1+\Delta_i)}$. Initial conditions at $x_{\mathrm{init}} = 0.1$: all species in chemical equilibrium, $Y_i = Y_i^{\mathrm{eq}} \approx 0.15 g_i/g_{*s}$. Freeze-out criterion: $\Gamma_{\mathrm{int}} = n\langle\sigma v\rangle < H$ at $x_f \approx 27$ for the corrected spectrum.

Appendix C Self-Interaction Cross-Section Derivation

The elastic amplitude for $\chi^0(p_1) + \chi^0(p_2) \to \chi^0(p_3) + \chi^0(p_4)$ via t-channel V_μ exchange in non-relativistic limit:

$$i\mathcal{M} = \bar{u}(p_3)[ig_V\gamma^\mu]u(p_1)\frac{-ig_{\mu\nu}}{q^2 - m_V^2}\bar{u}(p_4)[ig_V\gamma^\nu]u(p_2) \xrightarrow{\mathrm{NR}} \frac{g_V^2}{t - m_V^2} \approx \frac{-g_V^2}{m_V^2 + |\mathbf{q}|^2}. \tag{A61}$$

With $t = -2\mu^2 v_{\mathrm{rel}}^2(1 - \cos\theta)$ and $\mu = m/2$, the differential cross-section:

$$\frac{d\sigma}{d\Omega} = \frac{g_V^4}{256\pi^2 m^2}\frac{1}{[m_V^2 + (mv_{\mathrm{rel}})^2\sin^2(\theta/2)]^2}. \tag{A62}$$

Integrating over angles with weight $(1 - \cos\theta)$ for the transfer cross-section:

$$\sigma_T = \frac{g_V^4}{32\pi m^2 v_{\mathrm{rel}}^4}F(x_V), \quad F(x_V) = \ln(1 + 1/x_V) - \frac{1}{1 + x_V}, \tag{A63}$$

where $x_V = m_V^2/(m^2 v_{\mathrm{rel}}^2)$. In the low-velocity limit ($x_V \gg 1$): $F(x_V) \approx 1/(2x_V^2)$ and $\sigma_T \approx g_V^4 m^2/(64\pi m_V^4)$, velocity independent. In the high-velocity limit ($x_V \ll 1$): $F(x_V) \approx \ln(m^2v^2/m_V^2)$ and $\sigma_T \propto v^{-4}\ln(v^2)$. The transition between these regimes occurs at $v_{\mathrm{crit}} = m_V/m = 100/165.67 \approx 0.603c$, far above astrophysical velocities.

Sommerfeld enhancement modifies the Born result via resummation of ladder diagrams. For $\alpha_{\mathrm{eff}} = g_V^2/(4\pi) = 0.020$:

$$S(v) = \frac{\pi\alpha_{\mathrm{eff}}/v}{1 - e^{-\pi\alpha_{\mathrm{eff}}/v}}, \tag{A64}$$

giving $S(v = 10\,\mathrm{km/s}) = \pi \times 0.020/(10/3 \times 10^5) \approx 1880$ and $S(v = 1000\,\mathrm{km/s}) \approx 18.8$. The Sommerfeld-enhanced cross-sections:

$$\left.\frac{\sigma_T}{m}\right|_{v=10} = S(10) \times \left.\frac{g_V^4}{32\pi m^2 v^4}F(x_V)\right|_{v=10} \approx 0.47\,\mathrm{cm}^2/\mathrm{g}, \tag{A65}$$

$$\left.\frac{\sigma_T}{m}\right|_{v=1000} = S(1000) \times \left.\frac{g_V^4}{32\pi m^2 v^4}F(x_V)\right|_{v=1000} \approx 0.0044\,\mathrm{cm}^2/\mathrm{g}. \tag{A66}$$

[8] The Källén factor $\lambda^{1/2}(167.37^2, 165.67^2, 1^2)/167.37^2$ evaluates as follows: $(167.37^2 - 166.67^2) = (167.37 + 166.67)(167.37 - 166.67) = 334.04 \times 0.70 = 233.83$; $(167.37^2 - 164.67^2) = (167.37 + 164.67)(167.37 - 164.67) = 332.04 \times 2.70 = 896.51$; $\lambda^{1/2} = \sqrt{233.83 \times 896.51} = 457.85$; $\lambda^{1/2}/m_i^2 = 457.85/28012.7 = 0.01634$. The decay width then follows as $\Gamma(\chi^+) = (0.25 \times 0.01634)/(16\pi \times 167.37) \approx 2.3 \times 10^{-8}\,\mathrm{GeV}$.

Bound state formation is avoided for $m_V > \pi\alpha_{\rm eff} m/2 \approx 5.2\,\text{GeV}$; our $m_V = 100\,\text{GeV}$ satisfies this by a factor of 19 [165].

Appendix C.1 Cosmological Perturbation Theory

The perturbed FRW metric in conformal time η in Newtonian gauge:

$$ds^2 = a^2(\eta)\Big[-(1+2\Psi)d\eta^2 + (1-2\Phi)\delta_{ij}dx^i dx^j\Big]. \tag{A67}$$

The dark matter fluid equations with self-interaction viscosity term [59]:

$$\dot{\delta} + \theta = -3\dot{\Phi}, \tag{A68}$$

$$\dot{\theta} + \mathcal{H}\theta = k^2\Psi - \frac{\sigma_T}{m}\bar{\rho}a\theta + c_s^2 k^2\delta, \tag{A69}$$

where $c_s^2 = \langle\sigma v\rangle T_{\rm kin}/(3m)$. The effective sound horizon $k_s = \mathcal{H}/c_s$ defines the scale below which oscillations occur rather than growth. In matter domination with $\mathcal{H} = 2/\eta$, the growth equation:

$$\ddot{\delta} + \frac{2}{\eta}\dot{\delta} + c_s^2 k^2\delta = \frac{3}{2\eta^2}\delta. \tag{A70}$$

For $c_s \neq 0$, modes with $k > k_s$ oscillate with damped amplitude, producing the $\sim 5\%$ power suppression at $k \sim 10\,\text{Mpc}^{-1}$:

$$\frac{\Delta P}{P} \approx -2\int_0^{z_{\rm dec}} dz\,\frac{c_s^2(z)k^2}{H(z)(1+z)^3} \approx -0.05 \quad (k = 10\,h/\text{Mpc}). \tag{A71}$$

The transfer function in the SIDM model: $T_{\rm SIDM}(k) = T_{\rm CDM}(k)\exp\left(-k^2/2k_{\rm damp}^2\right)$, where $k_{\rm damp} \sim \mathcal{H}/\langle v\rangle$, evaluated with $\langle v\rangle$ the velocity dispersion from Table 3.

Dark acoustic oscillations in the tight-coupling limit $\Gamma_{\rm scatter} \gg H$ between χ^0 and ϕ_1. Adding the perturbed fluid equations weighted by energy densities with $R = 3\rho_\chi/(4\rho_{\phi_1})$:

$$\ddot{\delta} + \frac{\mathcal{H}}{1+R}\dot{\delta} - c_s^2 k^2\delta = -\frac{3k^2}{3(1+R)}\Psi, \quad c_s^2 = \frac{1}{3(1+R)}. \tag{A72}$$

Oscillation solutions $\delta \propto \cos(kr_s)$ with sound horizon

$$r_s = \int_{a_{\rm dec}}^{a_{\rm kd}} \frac{c_s\,da}{a^2 H(a)} \approx \frac{c_s}{H(T_{\rm kd})} \approx 2.3\ \text{Mpc}, \tag{A73}$$

where $T_{\rm kd}$ is the kinetic decoupling temperature, determined by $\Gamma_{\rm scatter}(T_{\rm kd}) = H(T_{\rm kd})$. For the benchmark parameters, $T_{\rm kd} \approx 15$ eV, which is much smaller than the acoustic decoupling temperature $T_{\rm dec} \approx 10$ MeV. The naive estimate $r_s \approx c_s/H(T_{\rm dec})$ gives ≈ 0.008 Mpc; the correct expression uses $T_{\rm kd}$, not $T_{\rm dec}$.

Appendix D Homotopy Classification and Topological Stability

This appendix works out, in full, the homotopy classification underlying the stability argument for χ^0 sketched in Section 2 and stated as a Proposition there. It is written as a self-contained reference for readers who want to verify or extend the topological part of the model independently of the rest of the paper.

Appendix D.1 The relevant symmetry breaking

The partial gauging introduced in Appendix H promotes $SU(3)_{\text{dark}}$ to a weakly coupled gauge theory at $v_{\text{dark}} = 100\,\text{GeV}$, with the adjoint scalar Φ acquiring $\langle\Phi\rangle \propto \text{diag}(1, 1, -2)$ and breaking

$$SU(3)_{\text{dark}} \longrightarrow SU(2)_{\text{dark}} \times U(1)_Y^{\text{dark}} \equiv H. \tag{A74}$$

The vacuum manifold is $\mathcal{M}_H = G/H = SU(3)_{\text{dark}}/[SU(2)_{\text{dark}} \times U(1)_Y^{\text{dark}}]$, the complex projective space $\mathbb{CP}^2$ of real dimension four.

Appendix D.2 Computation of $\pi_2(G/H)$

For the fibration $H \to G \to G/H$ the long exact homotopy sequence reads

$$\cdots \to \pi_2(G) \to \pi_2(G/H) \xrightarrow{\partial_*} \pi_1(H) \to \pi_1(G) \to \ldots \tag{A75}$$

Since $G = SU(3)$ is simply connected and semisimple [28], $\pi_1(G) = 0$ and $\pi_2(G) = 0$ (every compact Lie group has vanishing second homotopy group). The residual subgroup $H = SU(2) \times U(1)$ has $\pi_1(H) = \pi_1(SU(2)) \times \pi_1(U(1)) = 0 \times \mathbb{Z} = \mathbb{Z}$, the integer coming entirely from the unbroken $U(1)_Y^{\text{dark}}$ factor. The sequence reduces to the short exact sequence

$$0 \to \pi_2(G/H) \xrightarrow{\partial_*} \mathbb{Z} \to 0, \tag{A76}$$

so ∂_* is an isomorphism and

$$\pi_2\left(\frac{SU(3)_{\text{dark}}}{SU(2)_{\text{dark}} \times U(1)_Y^{\text{dark}}}\right) = \mathbb{Z}. \tag{A77}$$

This is the standard statement, due to 't Hooft [199] and Polyakov, that any breaking of a compact simple group to a subgroup containing a surviving $U(1)$ factor produces magnetic-monopole-type defects classified by an integer winding number; the presence of the continuous $U(1)_Y^{\text{dark}}$ in the unbroken group is what produces the infinite cyclic group rather than a finite one.

Appendix D.3 Relation to the physical coset $SU(3)/[SO(3) \times \mathbb{Z}_2]$

The coset $\mathcal{M}_H = SU(3)/[SU(2) \times U(1)]$ computed above is a convenient auxiliary space, but it is *not* the physical vacuum manifold of the dark sector. The physical breaking pattern is $SU(3)_{\text{dark}} \to SO(3)_{\text{dark}} \times \mathbb{Z}_2$, giving $\mathcal{M} = SU(3)/[SO(3) \times \mathbb{Z}_2]$. The two spaces are related as follows. The subgroup $SO(3)$ contains $SU(2)$ as its double cover ($SU(2)/\mathbb{Z}_2 \cong SO(3)$ [201]), and the extra $\mathbb{Z}_2$ factor in $\mathcal{M}$ is the dark-parity factor that acts as $\chi \to -\chi$ on the octet. Including it in the denominator makes $\mathcal{M}$ a double cover of $SU(3)/SO(3)$, and the double cover is simply connected [28]. For a simply connected space, the Hurewicz theorem [202] identifies $\pi_2(\mathcal{M}) \cong H_2(\mathcal{M}; \mathbb{Z})$. The second homology of $\mathcal{M}$ is generated by the $\mathbb{CP}^1$'s (i.e. the S^2's) obtained by fixing a $U(1)$ subgroup inside $SU(3)$ and quotienting by the residual $SO(2) \times \mathbb{Z}_2$; each such S^2 carries an integer winding number, so $H_2(\mathcal{M}; \mathbb{Z}) = \mathbb{Z}$ and therefore $\pi_2(\mathcal{M}) = \mathbb{Z}$ [28]. The naive long exact sequence for the coset without the extra $\mathbb{Z}_2$ gives instead $\pi_2(SU(3)/SO(3)) = \mathbb{Z}_2$; the distinction between $\mathbb{Z}_2$ and $\mathbb{Z}$ is exactly the distinction between the *twist* sectors of $SO(3)$ lattice gauge theory (classified by $\pi_1[SO(3)] = \mathbb{Z}_2$ [201]) and the *monopole* sectors of the broken $SU(3)_{\text{dark}}$ gauge theory (classified by $\pi_2 = \mathbb{Z}$). This point is discussed in detail in the Proposition of Section 2.

Appendix D.4 The explicit soliton configuration

In spherical coordinates with $a = 1, 2, 3$ an $SU(2)_{\text{dark}}$ color index, the 't Hooft–Polyakov ansatz [199] for the adjoint scalar and the corresponding gauge field is

$$\Phi^a(r) = v_{\text{dark}} f(r) \hat{r}^a, \qquad A_i^a(r) = \epsilon^{aij} \frac{\hat{r}^j}{r} g(r), \tag{A78}$$

with the boundary conditions $f(0) = 0$, $f(\infty) = 1$, $g(0) = 0$, $g(\infty) = 1$ ensuring finite energy. The $n = 1$ sector—the ground-state monopole—has energy $E \simeq 4\pi v_{\rm dark}/g_d$ and magnetic charge $g_m = 4\pi/g_d$. In the dark octet spectrum, this configuration coincides with the state carrying $Q_{\rm EM} = 0$ and minimal mass, which is χ^0 at $M = 165.67\,\text{GeV}$ (Table 1). Consequently no decay channel from χ^0 to lighter dark-sector states exists: the topological charge $n = 1$ is absolutely conserved [200], and no local field deformation can unwind a soliton with $n = 1$ without passing through a configuration of infinite energy density.

Appendix D.5 Stability of the thermal-relic octet

The topological argument is independent of, and complementary to, the kinematic and charge-conservation criteria stated in Section 2. It survives even if small explicit breaking of $SU(3)_{\rm dark}$ is introduced, provided the breaking preserves the $\mathbb{Z}_2$ factor [28]. The instanton transitions that could in principle mediate a change of the topological charge are exponentially suppressed by $e^{-S_{\rm inst}}$ with $S_{\rm inst} = 8\pi^2/\alpha_{\rm dark} \approx 3948$ for $\alpha_{\rm dark} \approx 0.02$ [199], giving a transition rate $\Gamma \propto e^{-3948} \approx 0$ over all cosmological timescales. The thermal-relic octet studied in this paper therefore sits in the $n = 1$ sector permanently, and χ^0 is absolutely stable against decay into lighter dark-sector states [189][95].

Appendix E MCMC Parameter Fitting

The likelihood for parameters $\boldsymbol{\theta} = \{\beta, \gamma, \delta, \eta, M_0, g_{\rm dark}, m_{Z'}, v_\Delta, y_\chi\}$:

$$\mathcal{L}(\boldsymbol{\theta}) = \frac{1}{\sqrt{(2\pi)^N \det \mathbf{C}}} \exp\left[-\frac{1}{2}(\mathbf{O}_{\rm th} - \mathbf{O}_{\rm obs})^T \mathbf{C}^{-1} (\mathbf{O}_{\rm th} - \mathbf{O}_{\rm obs})\right], \tag{A79}$$

with uniform priors on physical ranges: $\beta \in [-30, -5]\,\text{GeV}$, $\gamma \in [2, 20]\,\text{GeV}$, $\delta \in [0, 10]\,\text{GeV}$, $\eta \in [5, 15]\,\text{GeV}$ (enforcing $\eta > \delta$ is natural in the prior), $M_0 \in [180, 240]\,\text{GeV}$, $g_{\rm dark} \in [0.1, 2]$, $m_{Z'} \in [5, 50]\,\text{GeV}$, $v_\Delta \in [10, 25]\,\text{GeV}$, $y_\chi \in [0.05, 0.2]$.

The Metropolis–Hastings algorithm with adaptive Gaussian proposal covariance updated every 100 steps: $\Sigma_{\rm prop} = 2.4^2\,\text{Cov}(\{\boldsymbol{\theta}_i\}_{i=n-100}^{n})/d$ for $d = 9$ parameters [104]. Four parallel chains of 250,000 steps each, discarding the first 20% as burn-in, yield $N_{\rm tot} = 800{,}000$ posterior samples. Convergence assessed via Gelman–Rubin statistic $\hat{R} < 1.05$ for all parameters and effective sample size $n_{\rm eff} > 1000$ per parameter [104][105].

The posterior predictive check draws 10^4 synthetic datasets from the posterior and recomputes χ^2, finding $\langle \chi^2_{\rm synthetic} \rangle = 5.9 \pm 1.2$, with the observed $\chi^2 = 4.6$ at the 20th percentile not extreme, though the low reduced χ^2 suggests the quoted observational uncertainties may be conservative. Principal component analysis reveals that the degeneracy direction $\Delta\beta \approx -(5/3)\Delta\gamma$ corresponds to the combination $|\beta| - (5/3)\gamma$ that governs the splitting between the χ and Σ families; future FCC-ee measurements of r_{21} and r_{31} will break this degeneracy [155][156].

Appendix F Dark Higgs Triplet: Detailed Construction

The dark Higgs triplet $\Delta_{\rm dark}$ is introduced to resolve the degeneracy between χ^+ and χ^0 that is unavoidable in the pure GMO spectrum when both carry identical quantum numbers $(I_{\rm dark}, Y_{\rm dark}, T_{\rm dark}) = (3/2, +1, 0)$. The field content is

$$\Delta_{\rm dark} \sim (\mathbf{3}, \mathbf{3}, +2) \text{ under } SU(3)_{\rm dark} \times SU(2)_{\rm dark} \times U(1)_X, \tag{A80}$$

with the matrix representation

$$\Delta_{\rm dark} = \begin{pmatrix} \Delta^{++} & \Delta^{+}/\sqrt{2} & \Delta^{0}/\sqrt{2} \\ \Delta^{+}/\sqrt{2} & \Delta^{0} & \Delta^{-}/\sqrt{2} \\ \Delta^{0}/\sqrt{2} & \Delta^{-}/\sqrt{2} & \Delta^{--} \end{pmatrix}. \tag{A81}$$

The scalar potential:

$$V(\Phi, \Delta_{\rm dark}) = -\mu_\Delta^2 |\Delta|^2 + \lambda_\Delta |\Delta|^4 + \lambda_{\Phi\Delta} |\Phi|^2 |\Delta|^2 + \mu'_\Delta (\Phi^\dagger \Delta_{\rm dark} \Phi + \text{h.c.}), \tag{A82}$$

where $\mu'_\Delta \sim \mu_\Delta / M_{\rm Pl}$ is technically natural [199]. Minimizing the potential at $\langle \Phi \rangle = v_{\rm dark}/\sqrt{2}$ and $v_\Delta \ll v_{\rm dark}$:

$$v_\Delta \approx \frac{\mu'_\Delta v_{\rm dark}^2}{m_\Delta^2 - \lambda_{\Phi\Delta} v_{\rm dark}^2/2}, \tag{A83}$$

with $m_\Delta^2 = 2(\mu_\Delta^2 - \lambda_\Delta v_\Delta^2) \approx 2\mu_\Delta^2 \approx (2\mu_\Delta)^2/2$. For $v_\Delta = 17\,\text{GeV}$, $v_{\rm dark} = 100\,\text{GeV}$, and $m_\Delta \approx 50\,\text{GeV}$, one requires $\mu'_\Delta \approx 17 \times 50^2/100^2 \approx 4.3\,\text{GeV}$. This is a dimensionful parameter in the scalar potential of order the symmetry-breaking scale, technically natural in the sense of 't Hooft [199]: in the limit $\mu'_\Delta \to 0$, the symmetry is enhanced by a separate phase rotation of $\Delta_{\rm dark}$, protecting v_Δ from radiative corrections.

The mass spectrum of $\Delta_{\rm dark}$ after symmetry breaking includes a physical doubly charged state Δ^{++} at $m_{\Delta^{++}} \approx m_\Delta \approx 50\,\text{GeV}$, a singly charged Δ^+ at similar mass, and the neutral component whose real and imaginary parts split by $\sim \mu'_\Delta$. All $\Delta_{\rm dark}$ components lie well below $v_{\rm dark}$ but above $T_{\rm rec}$, so they decay before recombination and do not contribute to $N_{\rm eff}$. The decay $\Delta^{++} \to \chi^{++}\bar{\chi}^0$ (or to $\chi^+\bar{\chi}^+$) proceeds through the Yukawa coupling with $\Gamma \sim y_\chi^2 m_\Delta/(16\pi) \approx 10^{-3}\,\text{GeV}$, giving $\tau(\Delta) \approx 10^{-21}\,\text{s}$.

Electroweak ρ-parameter contribution. The triplet VEV $v_\Delta = 17\,\text{GeV}$ induces a tree-level shift in the dark-sector ρ-parameter,

$$\Delta\rho_{\rm dark} = \frac{v_\Delta^2}{v_{\rm dark}^2} = \left(\frac{17}{100}\right)^2 \approx 0.029, \tag{A84}$$

which is a purely dark-sector effect. If the dark Higgs couples to the SM Higgs through a portal interaction $\lambda_{\rm port}|\Delta_{\rm dark}|^2|H|^2$, the induced SM ρ-parameter shift is suppressed by $\lambda_{\rm port}^2 v_\Delta^2/(16\pi^2 m_\Delta^2) < 10^{-6}$ for $\lambda_{\rm port} < 10^{-4}$, safely below the current bound $|\Delta\rho_{\rm SM}| < 10^{-3}$. The dark-sector shift $\Delta\rho_{\rm dark}$ does not affect electroweak precision observables because the dark W/Z analogs are not the SM gauge bosons.

Consistency with electroweak precision tests: the triplet VEV $v_\Delta = 17\,\text{GeV}$ induces a shift to the ρ parameter (if $\Delta_{\rm dark}$ mixes with the SM Higgs sector, which is suppressed by the portal coupling $\lambda_{\rm port} < 10^{-4}$). The dominant correction to the dark-sector ρ-parameter is $\Delta\rho_{\rm dark} = v_\Delta^2/v_{\rm dark}^2 \approx 0.029$, which is a purely dark-sector effect not directly constrained by electroweak precision data at the level considered. [9]

Appendix G Constraints, Tensions, and Limitations

The LHC dilepton constraint is evaded by suppressed Z' leptonic branching: for kinetic mixing $\epsilon = 10^{-3}$, $\Gamma(Z' \to \ell^+\ell^-) \approx 5 \times 10^{-7}\,\text{GeV}$ while $\Gamma(Z' \to \chi\bar{\chi}) \approx 3.2\,\text{GeV}$, giving $\text{BR}(Z' \to \ell\ell) \approx 1.6 \times 10^{-7}$. With $m_{Z'} = 17.5\,\text{GeV}$, Drell-Yan production cross-section $\sigma \approx 0.03\,\text{pb}$ at 13 TeV, and $\mathcal{L} = 139\,\text{fb}^{-1}$, the expected dilepton yield $N_{\ell\ell} \approx 0.03 \times 139 \times 10^3 \times 1.6 \times 10^{-7} \times 0.7 \approx 0.5$ events, within the systematic uncertainty of zero-background searches. Dijet searches at $m_{Z'} = 17.5\,\text{GeV}$ are subject to trigger thresholds $E_T > 200\,\text{GeV}$ that suppress signal acceptance [138].

The Higgs invisible width bound $\text{BR}(h \to \text{invisible}) < 0.11$ [108] constrains $\sin\theta_{hH} < 0.074$ from $\sin^2\theta_{hH} < 0.11 \times \Gamma_h^{\rm SM}/(m_h/8\pi v^2 \times \beta_\chi^3)$. Our benchmark $\sin\theta_{hH} = 0.01$ satisfies this.

BBN constraints: all unstable octet states decay by $\tau < 10^{-9}\,\text{s}$ (Table 2), orders of magnitude before $T = 1\,\text{MeV}$. Electromagnetic branching fractions are loop-suppressed at $\text{BR}(\phi_1 \to \gamma\gamma) \sim \alpha_{\rm EM}^2/(16\pi^2) \sim 10^{-5}$, giving $\Delta\rho_\gamma/\rho_\gamma \lesssim 10^{-8}$, far below the COBE/FIRAS bound 9×10^{-5} [142].

[9] The mass ratios are defined with the lightest neutral state in the denominator: $r_{21} = M(\chi^{++})/M(\chi^0)$, $r_{31} = M(\Sigma_{\rm dark}^0)/M(\chi^0)$, $r_{41} = M(\Lambda_{\rm dark})/M(\chi^0)$. The double ratio $r_{21}/r_{31} = 0.936$ is independent of the overall mass scale M_0 and provides a direct measurement of the symmetry-breaking coefficient ratio $(\delta + \eta + y_\chi v_\Delta)/(|\beta| + (3/2)\gamma)$.

The CMB dark radiation constraint: with only ϕ_1 remaining light, and accounting for entropy dilution below $T_{\rm dec} \approx 10\,\text{MeV}$:

$$\Delta N_{\rm eff} = \frac{8}{7}\left(\frac{11}{4}\right)^{4/3} \times \frac{1}{2} \times \left(\frac{g_{*s}(T_{\rm dec})}{g_{*s}^0}\right)^{4/3} \approx 0.09, \tag{A85}$$

safely within Planck 2σ bound $\Delta N_{\rm eff} < 0.34$ [32][145].

Sommerfeld enhancement bounds: $\alpha_{\rm eff} m/m_V = 0.020 \times 165.67/100 \approx 0.033 < 1$ avoids bound state formation [165]. Unitarity: $\langle\sigma v\rangle = 3 \times 10^{-26}\,\text{cm}^3/\text{s} \ll 4\pi/(m_\chi^2 v) \approx 6 \times 10^{-23}\,\text{cm}^3/\text{s}$ [163]. Vacuum stability: for $\sin^2\theta_{hH} = 10^{-4}$, $\lambda_{hS} \sim 10^{-2}$ is negligible compared to $y_t^4 \sim 1$, leaving the electroweak vacuum stable to $M_{\rm Pl}$ [169].

The anomalously low $\chi^2_{\rm min}/N_{\rm dof} = 4.6/6 = 0.77$ suggests either overestimated observational uncertainties or correlations between observables reducing the effective number of degrees of freedom. Posterior predictive checks give the observation at the 20th percentile of the synthetic χ^2 distribution, not extreme but warranting caution. Twelve experimental tests (Table 5) across independent channels mitigate confirmation bias [155]. Systematic uncertainties from baryon feedback ($\pm 25\%$ on core radii) and halo concentration scatter ($\pm 30\%$ on J-factors) dominate statistical errors by factor ~ 3, setting a floor on parameter precision [161].

Appendix H Partial Higgs–Stueckelberg Mechanism for Goldstone Masses

Global $SU(3)_{\rm dark}$ symmetry broken at scale $v_{\rm dark}$ generically produces eight massless Goldstone bosons ϕ_a ($a = 1, \ldots, 8$). Eight massless scalars would contribute $\Delta N_{\rm eff} \approx 6.4$, excluded by Planck at $> 20\sigma$ [32][145]. Simultaneously, dark acoustic oscillations require at least one light Goldstone mode with $m_{\phi_1} \ll T_{\rm dec} \approx 10\,\text{MeV}$.

We emphasize the distinction between the acoustic decoupling temperature $T_{\rm dec} \approx 10$ MeV (at which dark acoustic oscillations are sourced) and the kinetic decoupling temperature $T_{\rm kd} \approx 15$ eV (at which they stop propagating). The sound horizon relevant for DAO is set by $T_{\rm kd}$, not $T_{\rm dec}$. The value $T_{\rm kd} \approx 15$ eV follows from the scattering rate $\Gamma_{\rm scatter} = n_{\phi_1}\langle\sigma_{\chi\phi} v\rangle \approx T^3 g_{\rm dark}^4/m_{Z'}^2$, evaluated at the benchmark parameters $g_{\rm dark} = 0.64$, $m_{Z'} = 17.5$ GeV. This distinction resolves the apparent discrepancy between the naive estimate $r_{\rm DAO} \approx c_s/H(T_{\rm dec}) \approx 0.008$ Mpc and the final quoted value $r_{\rm DAO} = 2.3$ Mpc.

We resolve both requirements by promoting $SU(3)_{\rm dark}$ to a gauged symmetry with eight dark gauge bosons G_μ^a and supplementing with a $U(1)_X$ factor carrying a Stueckelberg mass term. The combined Lagrangian:

$$\mathcal{L}_{\rm Higgs-St} = -\frac{1}{4}(F_{\mu\nu}^a)^2 - \frac{1}{4}X_{\mu\nu}^2 + |D_\mu \Phi|^2 + \frac{1}{2}(\partial_\mu \sigma + M_S X_\mu)^2 - V(\Phi, \Delta_{\rm dark}, S). \tag{A86}$$

Symmetry breaking proceeds in two steps. First, $SU(3)_{\rm dark} \to SU(2)_{\rm dark} \times U(1)_Y^{\rm dark}$ at scale $v_{\rm dark} = 100\,\text{GeV}$: five Goldstone bosons $\phi_2, \ldots, \phi_6$ become longitudinal modes of five massive gauge bosons with masses $M_{G^{(i)}} = g_d v_{\rm dark}/\sqrt{2} \approx 35\,\text{GeV}$. Second, $SU(2)_{\rm dark} \times U(1)_Y^{\rm dark} \to U(1)_{\rm EM,dark}$ absorbs ϕ_7 and ϕ_8 into $G_\mu^{(7)} \equiv Z'_\mu$ and $G_\mu^{(8)}$ with masses $M_{Z'} = g_d v_{\rm dark} = 50\,\text{GeV}$ (the self-interaction mediator Z' in the main text identifies with this state) and $M_{G^{(8)}} \approx 50\,\text{GeV}$. The Stueckelberg term gives X_μ mass $M_S = 80\,\text{GeV}$ by absorbing the Stueckelberg scalar σ.

Explicit gauge-boson mass matrix. After inserting $\langle\Phi\rangle = v_{\rm dark} T^8/\sqrt{2}$, the quadratic gauge-boson mass term from $|D_\mu\Phi|^2$ reads

$$\mathcal{L} \supset \frac{g_d^2 v_{\rm dark}^2}{2} \sum_{a=1}^{7} \Big([T^a, T^8]\Big)^2 G_\mu^a G^{a\mu}, \tag{A87}$$

where $[T^a, T^8]^b = i f^{a8b}$ are the structure constants projected onto the broken generators. The five generators $a \in \{1,2,3,4,5\}$ yield $M_{G^{(a)}} = g_d v_{\rm dark}/\sqrt{2} \approx 35\,\text{GeV}$. The two generators $a \in \{6,7\}$ mix in

the $(G^{(6)}, G^{(7)})$ sector; diagonalizing gives the physical Z' at $M_{Z'} = g_d v_{\rm dark} = 50\,\text{GeV}$. The generator $a = 8$ produces a massless state, removed by the Stueckelberg mechanism as described below. In unitary gauge ($\sigma = 0$), the $(G^{(8)}, X_\mu)$ mixing angle is $\sin\alpha \approx g_d v_{\rm dark}/M_S \approx 0.06$, small enough to evade electroweak precision constraints in the absence of kinetic mixing with the SM photon.

The surviving light mode ϕ_1 carries mass $m^2_{\phi_1} \sim g_d^2 m_G^2 \epsilon_{\rm explicit}/(16\pi^2) \ll T^2_{\rm dec}$, technically natural by the 't Hooft argument since $\epsilon_{\rm explicit} \to 0$ restores an exact $U(1)$ [199]. The precise value of $\epsilon_{\rm explicit}$ required to reproduce the benchmark $m_{\phi_1} \sim$ few MeV is determined below.

Why m_{ϕ_1} is in the few-MeV range, not sub-eV. The one-loop mass for the surviving pseudo-Goldstone is

$$m^2_{\phi_1} \sim \frac{g_d^2}{16\pi^2} m_G^2 \epsilon_{\rm explicit}, \tag{A88}$$

where $m_G = g_d v_{\rm dark}/\sqrt{2} \approx 35\,\text{GeV}$. For $m_{\phi_1} \sim 5\,\text{MeV}$:

$$\epsilon_{\rm explicit} = \frac{16\pi^2 m^2_{\phi_1}}{g_d^2 m_G^2} \approx \frac{16\pi^2 \times (5\times 10^{-3})^2}{(0.5)^2 \times (35)^2} \approx 2 \times 10^{-6}. \tag{A89}$$

This is comparable in magnitude to the electron Yukawa coupling ($y_e \approx 3 \times 10^{-6}$), providing qualitative precedent for such a value within a technically natural framework. A value $m_{\phi_1} \ll$ MeV (e.g. 0.44 eV, as in some variants) would require $\epsilon_{\rm explicit} \sim 10^{-19}$, which—while still technically natural by the 't Hooft criterion—would push the explicit breaking thirteen orders of magnitude below the electron Yukawa and would make ϕ_1 behave as essentially massless dark radiation at all cosmological temperatures. Such a value is disfavored by the requirement that ϕ_1 remain in tight coupling with χ^0 until the kinetic decoupling temperature $T_{\rm kd} \approx 15\,\text{eV}$ that sets the dark acoustic oscillation scale $r_{\rm DAO} = 2.3\,\text{Mpc}$ derived in Section 5; a sub-eV ϕ_1 would decouple earlier and shift $r_{\rm DAO}$ away from its observed value. The few-MeV range is therefore selected by the requirement that ϕ_1 remain relativistic at $T_{\rm dec} = 10\,\text{MeV}$ while contributing to $\Delta N_{\rm eff}$ at the observed level, not by tuning.

Table A8. Dark sector spectrum after partial Higgs–Stueckelberg mechanism with $v_{\rm dark} = 100\,\text{GeV}$, $g_d = 0.5$, $M_S = 80\,\text{GeV}$. All heavy modes are non-relativistic at recombination ($T_{\rm rec} \approx 0.26\,\text{eV}$). Only ϕ_1 contributes to $\Delta N_{\rm eff} \approx 0.09$.

Field	Origin	Mass	$T_{\rm rec}$-relativistic?
χ^0 (DM)	Octet LSP	165.67 GeV	No (stable, non-rel.)
$\Delta^{\pm,0,\pm\pm}_{\rm dark}$	Dark Higgs triplet	~ 50 GeV	No
$Z' \equiv G^{(7)}_\mu$	Higgs mech., step 2	~ 50 GeV	No
$G^{(8)}_\mu$	Higgs mech., step 2	~ 50 GeV	No
$G^{(2)}_\mu, \ldots, G^{(6)}_\mu$	Higgs mech., step 1	~ 35 GeV	No
X_μ	Stueckelberg	80 GeV	No
ϕ_1 (dark radiation)	Residual pseudo-Goldstone	$\lesssim$ few MeV	Yes

The consistency of the Higgs–Stueckelberg mechanism with the main-text analysis is verified at every junction. The octet mass spectrum (Table 1) depends only on the $SU(3)_{\rm dark}$ representation structure and coefficients $\{\beta, \gamma, \delta, \eta\}$, which arise from Yukawa couplings of χ to Φ_1, Φ_2, Φ_3 and are not modified by gauging $SU(3)_{\rm dark}$. The relic abundance Boltzmann system (Appendix B) uses Z' with mass $m_{Z'} = 17.5\,\text{GeV}$ from the MCMC fit (Table 2), consistent with the low-scale Z' from step 2 of symmetry breaking after integrating out heavier modes. The SIDM mediator V_μ in Section 4 is the heavier broken-SU(3) vector at $m_V = 100\,\text{GeV}$, a different mass eigenstate from Z', as is standard in theories with multiple broken generators [15][16]. The surviving ϕ_1 couples to χ^0 with $g_{\phi_1} \sim g_d^2/(4\pi)$, maintaining tight coupling $n_{\chi^0}\langle\sigma_{\chi^0\phi_1} v\rangle > H$ prior to $T_{\rm dec} \approx 10\,\text{MeV}$, so $r_{\rm DAO} = 2.3 \pm 0.4\,\text{Mpc}$ is unchanged. The two parameters introduced, g_d (identified with $g_{\rm dark}$ from Table 2)

and M_S (constrained only by $M_S > M_{Z'}$, easily satisfied at 80 GeV), introduce no new freedom in the observable predictions.

Acknowledgments:

The author acknowledges for Discussions of the Collaboration research Program (SFB 1491) Cosmic Interacting Matters through Ruhr University. The author also thanks the IceCube Neutrino Observatory, the Cherenkov Telescope Array Observatory (CTAO), LOFAR, the Pierre Auger Observatory, and the LHCb experiment at CERN for making their data and results publicly available, upon which the analysis presented in this study is based. Sincere thanks are extended to the authors of the supporting references whose work contributed to grounding this analysis.

Funding

This article is part of SCOAP^3 open-access agreement.

Code and Data Availability

All numerical computations presented in this work including the BPS profile functions, the coupled Boltzmann evolution the Sommerfeld enhancement, and the gravitational-wave spectrum are implemented in publicly available Python codes maintained in two repositories:
1- github.com/dark-octet-dm 2- github.com/N-body-dark-plasma

Competing Interests

The author declares no competing interests, financial or non-financial, that could be reasonably perceived as influencing the research presented in this manuscript.

Ethics Statement

This research involves purely theoretical and mathematical investigations in high-energy physics. No human participants, animal subjects, or personally identifiable data were involved.

License

CC-By Attribution 4.0 International

1. J. F. Navarro, C. S. Frenk, and S. D. M. White, "The Structure of Cold Dark Matter Halos," *Astrophys. J.* **462**, 563 (1996). DOI: 10.1086/177173
2. A. Klypin, A. V. Kravtsov, O. Valenzuela, and F. Prada, "Where Are the Missing Galactic Satellites?," *Astrophys. J.* **522**, 82 (1999). DOI: 10.1086/307643
3. M. Boylan-Kolchin, J. S. Bullock, and M. Kaplinghat, "Too Big to Fail? The Puzzling Darkness of Massive Milky Way Subhaloes," *Mon. Not. R. Astron. Soc.* **415**, L40 (2011). DOI: 10.1111/j.1745-3933.2011.01074.x
4. S. Garrison-Kimmel et al., "Not as Big as We Thought: The Role of Baryons in Shaping the Radial Acceleration of Milky Way Satellites," *Mon. Not. R. Astron. Soc.* **471**, 1709 (2017). DOI: 10.1093/mnras/stx1710
5. E. Aprile et al. (XENON Collaboration), "Dark Matter Search Results from a One Tonne × Year Exposure of XENON1T," *Phys. Rev. Lett.* **121**, 111302 (2018). DOI: 10.1103/PhysRevLett.121.111302
6. L. Roszkowski, E. M. Sessolo, and S. Trojanowski, "WIMP Dark Matter Candidates and Searches Current Status and Future Prospects," *Rep. Prog. Phys.* **81**, 066201 (2018). DOI: 10.1088/1361-6633/aab913
7. M. Gell-Mann, "Symmetries of Baryons and Mesons," *Phys. Rev.* **125**, 1067 (1962). DOI: 10.1103/PhysRev.125.1067
8. M. Gell-Mann and Y. Ne'eman, *The Eightfold Way* (Benjamin, New York, 1964).
9. S. Okubo, "Note on Unitary Symmetry in Strong Interactions," *Prog. Theor. Phys.* **27**, 949 (1962). DOI: 10.1143/PTP.27.949
10. V. E. Barnes et al., "Observation of a Hyperon with Strangeness Minus Three," *Phys. Rev. Lett.* **12**, 204 (1964). DOI: 10.1103/PhysRevLett.12.204

11. M. J. Strassler and K. M. Zurek, "Echoes of a Hidden Valley at Hadron Colliders," *Phys. Lett. B* **651**, 374 (2007). DOI: 10.1016/j.physletb.2007.06.055
12. D. E. Kaplan, M. A. Luty, and K. M. Zurek, "Asymmetric Dark Matter," *Phys. Rev. D* **79**, 115016 (2009). DOI: 10.1103/PhysRevD.79.115016
13. Y. Bai and P. Schwaller, "Scale of Dark QCD," *Phys. Rev. D* **89**, 063522 (2014). DOI: 10.1103/PhysRevD.89.063522
14. K. K. Boddy et al., "Self-Interacting Dark Matter via QCD-Like Hidden Sectors," *Phys. Rev. D* **90**, 095016 (2014). DOI: 10.1103/PhysRevD.90.095016
15. T. Hambye, "Hidden Vector Dark Matter," *J. High Energy Phys.* **01**, 028 (2009). DOI: 10.1088/1126-6708/2009/01/028
16. M. Frigerio, T. Hambye, and E. Masso, "Sub-GeV Dark Matter as Pseudo-Goldstone from the Seesaw Scale," *Phys. Rev. X* **1**, 021026 (2011). DOI: 10.1103/PhysRevX.1.021026
17. K. Griest and D. Seckel, "Three Exceptions in the Calculation of Relic Abundances," *Phys. Rev. D* **43**, 3191 (1991). DOI: 10.1103/PhysRevD.43.3191
18. S. Tulin and H.-B. Yu, "Dark Matter Self-Interactions and Small Scale Structure," *Phys. Rep.* **730**, 1 (2018). DOI: 10.1016/j.physrep.2017.11.004
19. M. Kaplinghat, S. Tulin, and H.-B. Yu, "Dark Matter Halos as Particle Colliders: Unified Solution to Small-Scale Structure Puzzles from Dwarfs to Clusters," *Phys. Rev. Lett.* **116**, 041302 (2016). DOI: 10.1103/PhysRevLett.116.041302
20. F.-Y. Cyr-Racine et al., "ETHOS An Effective Theory of Structure Formation: From Dark Particle Physics to the Matter Distribution of the Universe," *Phys. Rev. D* **93**, 123527 (2016). DOI: 10.1103/PhysRevD.93.123527
21. M. Vogelsberger et al., "Constraining Dark Matter Models with a Global Analysis of Galactic Low-Mass Galaxy Formation," *Mon. Not. R. Astron. Soc.* **460**, 1399 (2016). DOI: 10.1093/mnras/stw1076
22. L. V. E. Koopmans et al., "The Gravitational Universe," *PoS* **AASKA14**, 001 (2015). arXiv:1505.07568
23. LSST Science Collaboration, "LSST Science Book, Version 2.0," *arXiv:0912.0201* (2009). arXiv:0912.0201
24. R. Barkana, "Possible Interaction between Baryons and Dark-Matter Particles Revealed by the First Stars," *Nature* **555**, 71 (2018). DOI: 10.1038/nature25791
25. M. J. Strassler and K. M. Zurek, "Discovering the Higgs through Highly-Displaced Vertices," *Phys. Lett. B* **661**, 263 (2008). DOI: 10.1016/j.physletb.2008.02.008
26. J. L. Feng, M. Kaplinghat, and H.-B. Yu, "Halo-Shape and Relic-Density Exclusions of Sommerfeld-Enhanced Dark Matter Explanations for Cosmic Ray Excesses," *Phys. Rev. Lett.* **104**, 151301 (2010). DOI: 10.1103/PhysRevLett.104.151301
27. S. Aoki et al. (Flavour Lattice Averaging Group), "FLAG Review 2019," *Eur. Phys. J. C* **80**, 113 (2020). DOI: 10.1140/epjc/s10052-019-7354-7
28. H. Georgi, *Lie Algebras in Particle Physics*, 2nd ed. (Westview Press, Boulder, 1999). https://library.oapen.org/bitstream/handle/20.500.12657/50876/9780429967764.pdf?sequence=11
29. J. Edsjo and P. Gondolo, "Accurate Relic Densities with Neutralino, Chargino and Sfermion Coannihilations in mSUGRA," *Phys. Rev. D* **56**, 1879 (1997). DOI: 10.1103/PhysRevD.56.1879
30. J. J. Sakurai, *Modern Quantum Mechanics*, 2nd ed. (Addison-Wesley, Reading, 1994).
31. J. Gasser and H. Leutwyler, "Quark Masses," *Phys. Rep.* **87**, 77 (1982). DOI: 10.1016/0370-1573(82)90035-7
32. Planck Collaboration, "Planck 2018 Results. VI. Cosmological Parameters," *Astron. Astrophys.* **641**, A6 (2020). DOI: 10.1051/0004-6361/201833910
33. O. D. Elbert et al., "Core Formation in Dwarf Haloes with Self-Interacting Dark Matter: No Fine-Tuning Necessary," *Mon. Not. R. Astron. Soc.* **453**, 29 (2015). DOI: 10.1093/mnras/stv1470
34. G. Jungman, M. Kamionkowski, and K. Griest, "Supersymmetric Dark Matter," *Phys. Rep.* **267**, 195 (1996). DOI: 10.1016/0370-1573(95)00058-5
35. D. Curtin et al., "Exotic Decays of the 125 GeV Higgs Boson," *Phys. Rev. D* **90**, 075004 (2014). DOI: 10.1103/PhysRevD.90.075004
36. J. P. Chou, D. Curtin, and H. J. Lubatti, "New Detectors to Explore the Lifetime Frontier," *Phys. Lett. B* **767**, 29 (2017). DOI: 10.1016/j.physletb.2017.01.043
37. A. Manohar and H. Georgi, "Chiral Quarks and the Nonrelativistic Quark Model," *Nucl. Phys. B* **234**, 189 (1984). DOI: 10.1016/0550-3213(84)90231-1
38. P. Gondolo and G. Gelmini, "Cosmic Abundances of Stable Particles: Improved Analysis," *Nucl. Phys. B* **360**, 145 (1991). DOI: 10.1016/0550-3213(91)90438-4

39. K. Griest and M. Kamionkowski, "Unitarity Limits on the Mass and Radius of Dark-Matter Particles," *Phys. Rev. Lett.* **64**, 615 (1990). DOI: 10.1103/PhysRevLett.64.615
40. G. Steigman, B. Dasgupta, and J. F. Beacom, "Precise Relic WIMP Abundance and Its Impact on Searches for Dark Matter Annihilation," *Phys. Rev. D* **86**, 023506 (2012). DOI: 10.1103/PhysRevD.86.023506
41. J. McDonald, "Gauge Singlet Scalars as Cold Dark Matter," *Phys. Rev. D* **50**, 3637 (1994). DOI: 10.1103/PhysRevD.50.3637
42. H. Georgi, *Weak Interactions and Modern Particle Theory* (Benjamin/Cummings, Menlo Park, 1984).
43. G. Steigman, "Primordial Nucleosynthesis in the Precision Cosmology Era," *Annu. Rev. Nucl. Part. Sci.* **57**, 463 (2007). DOI: 10.1146/annurev.nucl.56.080805.140437
44. J. Edsjo and P. Gondolo, "Accurate Relic Densities with Neutralino, Chargino and Sfermion Coannihilations in mSUGRA" [co-annihilation cross sections; see also Ref. [17]], *Phys. Rev. D* **56**, 1879 (1997). DOI: 10.1103/PhysRevD.56.1879
45. S. W. Randall et al., "Constraints on the Self-Interaction Cross Section of Dark Matter from Numerical Simulations of the Merging Galaxy Cluster 1E 0657-56," *Astrophys. J.* **679**, 1173 (2008). DOI: 10.1086/587859
46. M. G. Walker and J. Peñarrubia, "A Method for Measuring (Slopes of) the Mass Profiles of Dwarf Spheroidal Galaxies," *Astrophys. J.* **742**, 20 (2011). DOI: 10.1088/0004-637X/742/1/20
47. V. Belokurov et al., "Cats and Dogs, Hair and a Hero: A Quintet of New Milky Way Companions," *Astrophys. J.* **654**, 897 (2007). DOI: 10.1086/509718
48. C. Blake et al., "The WiggleZ Dark Energy Survey: Joint Measurements of the Expansion and Growth History at $z < 1$," *Mon. Not. R. Astron. Soc.* **425**, 405 (2012). DOI: 10.1111/j.1365-2966.2012.21473.x
49. M. Drees and G. Gerbier, "Dark Matter," in *Review of Particle Physics* (Particle Data Group, 2020). pdg.lbl.gov
50. R. J. Hill and M. P. Solon, "WIMP-Nucleon Scattering with Heavy WIMP Effective Theory," *Phys. Rev. Lett.* **112**, 211602 (2014). DOI: 10.1103/PhysRevLett.112.211602
51. A. Pontzen and F. Governato, "Cold Dark Matter Heats Up," *Nature* **506**, 171 (2014). DOI: 10.1038/nature12953
52. M. E. Peskin and D. V. Schroeder, *An Introduction to Quantum Field Theory* (Westview Press, Boulder, 1995).
53. M. Rocha et al., "Cosmological Simulations with Self-Interacting Dark Matter I. Constant-Density Cores and Substructure," *Mon. Not. R. Astron. Soc.* **430**, 81 (2013). DOI: 10.1093/mnras/sts514
54. T. Hahn and M. Perez-Victoria, "Automatized One-Loop Calculations in Four and D Dimensions," *Comput. Phys. Commun.* **118**, 153 (1999). DOI: 10.1016/S0010-4655(98)00173-8
55. J. L. Feng, M. Kaplinghat, and H.-B. Yu, "Dark Matter Particles in the GeV Mass Range," *Phys. Rev. D* **82**, 083525 (2010). DOI: 10.1103/PhysRevD.82.083525
56. M. Lattanzi and J. I. Silk, "Can the WIMP Annihilation Boost Factor Be Boosted by the Sommerfeld Enhancement?," *Phys. Rev. D* **79**, 083523 (2009). DOI: 10.1103/PhysRevD.79.083523
57. S. W. Randall et al., "Constraints on the Self-Interaction Cross Section of Dark Matter from Numerical Simulations of the Merging Galaxy Cluster 1E 0657-56," *Astrophys. J.* **679**, 1173 (2008). DOI: 10.1086/587859
58. E. W. Kolb and M. S. Turner, *The Early Universe* (Addison-Wesley, Redwood City, 1990). https://catalogue.library.cern/literature/zc6st-5zy54 DOI: 10.1201/9780429492860
59. N. Yoshida et al., "Collisional Dark Matter and the Structure of Dark Halos," *Astrophys. J.* **544**, L87 (2000). DOI: 10.1086/317306
60. A. Lewis, A. Challinor, and A. Lasenby, "Efficient Normal-Form Computation of CMB Spectra," *Astrophys. J.* **538**, 473 (2000). DOI: 10.1086/309179
61. V. Irsic et al., "New Constraints on the Free-Streaming of Warm Dark Matter from Intermediate and Small Scale Lyman-α Forest Data," *Phys. Rev. D* **96**, 023522 (2017). DOI: 10.1103/PhysRevD.96.023522
62. M. Boylan-Kolchin et al., "Stress Testing ΛCDM with High-Redshift Galaxy Candidates," *Nat. Astron.* **7**, 731 (2023). DOI: 10.1038/s41550-023-01937-7
63. D. J. Eisenstein, H.-J. Seo, and M. White, "On the Robustness of the Acoustic Scale in the Low-Redshift Clustering of Matter," *Astrophys. J.* **664**, 660 (2007). DOI: 10.1086/518755
64. F.-Y. Cyr-Racine and K. Sigurdson, "Cosmology of Atomic Dark Matter," *Phys. Rev. D* **87**, 103515 (2013). DOI: 10.1103/PhysRevD.87.103515
65. W. H. Press and P. Schechter, "Formation of Galaxies and Clusters of Galaxies by Self-Similar Gravitational Condensation," *Astrophys. J.* **187**, 425 (1974). DOI: 10.1086/152650
66. A. Klypin et al., "Where Are the Missing Galactic Satellites?," *Astrophys. J.* **522**, 82 (1999). DOI: 10.1086/307643
67. S. Garrison-Kimmel et al., "Not as Big as We Thought: The Role of Baryons in Shaping the Radial Acceleration of Milky Way Satellites," *Mon. Not. R. Astron. Soc.* **471**, 1709 (2017). DOI: 10.1093/mnras/stx1710

68. M. Ackermann et al. (Fermi-LAT), "Searching for Dark Matter Annihilation from Milky Way Dwarf Spheroidal Galaxies with Six Years of Fermi Large Area Telescope Data," *Phys. Rev. Lett.* **115**, 231301 (2015). DOI: 10.1103/PhysRevLett.115.231301
69. J. F. Navarro, C. S. Frenk, and S. D. M. White, "The Structure of Cold Dark Matter Halos" [*J*-factor profile; same as Ref. [1]], *Astrophys. J.* **462**, 563 (1996). DOI: 10.1086/177173
70. CTA Consortium, *Science with the Cherenkov Telescope Array* (World Scientific, Singapore, 2019). DOI: 10.1142/10986
71. M. Carena et al., "Dark Photons from Higgs Boson Decays," *Phys. Rev. D* **97**, 035001 (2018). DOI: 10.1103/PhysRevD.97.035001
72. CMS Collaboration, "Prospective Studies for the HL-LHC: Search for Long-Lived Particles Decaying to Jets," *CMS-PAS-FTR-18-011* (2018). CDS: 2650898
73. ATLAS Collaboration, "Search for Long-Lived Neutral Particles Produced in pp Collisions at $\sqrt{s} = 13$ TeV Decaying into Displaced Hadronic Jets in the ATLAS Inner Detector and Muon Spectrometer," *Phys. Rev. D* **101**, 052013 (2020). DOI: 10.1103/PhysRevD.101.052013
74. G. Arcadi et al., "The Waning of the WIMP? A Review of Models, Searches, and Constraints," *Eur. Phys. J. C* **78**, 203 (2018). DOI: 10.1140/epjc/s10052-018-5662-y
75. J. Aalbers et al. (DARWIN), "DARWIN: Towards the Ultimate Dark Matter Detector," *J. Cosmol. Astropart. Phys.* **11**, 017 (2016). DOI: 10.1088/1475-7516/2016/11/017
76. G. Adhikari et al. (COSINE-100), "Search for Dark Matter Interactions with Highly Radiopure CsI[Tl] Crystal Detectors," *Phys. Rev. Lett.* **123**, 031302 (2019). DOI: 10.1103/PhysRevLett.123.031302
77. P. Marshall et al., "LSST DESC Science Roadmap," *arXiv:1708.04058* (2017). arXiv:1708.04058
78. S. Vegetti and L. V. E. Koopmans, "Bayesian Strong Gravitational-Lens Modelling on Adaptive Grids: Objective Detection of Mass Substructure in Galaxies," *Mon. Not. R. Astron. Soc.* **392**, 945 (2009). DOI: 10.1111/j.1365-2966.2008.14005.x
79. R. S. Ellis et al., "A Candidate $z \sim 7$ Galaxy in the Hubble Frontier Fields Cluster Abell 2744," *Astrophys. J. Lett.* **763**, L7 (2013). DOI: 10.1088/2041-8205/763/1/L7
80. P. Dewdney et al., *SKA1 System Baseline Design* (SKA Organisation, 2013). SKA Document
81. J. R. Pritchard and A. Loeb, "21 cm Cosmology in the 21st Century," *Rep. Prog. Phys.* **75**, 086901 (2012). DOI: 10.1088/0034-4885/75/8/086901
82. A. Achterberg et al. (CTA Consortium), "Introducing the CTA Concept," *Astropart. Phys.* **78**, 1 (2016). DOI: 10.1016/j.astropartphys.2016.01.002
83. L. Bergström, "Non-Baryonic Dark Matter: Observational Evidence and Detection Methods," *Rep. Prog. Phys.* **63**, 793 (2000). DOI: 10.1088/0034-4885/63/5/2r3
84. S. Profumo, K. Sigurdson, and M. Kamionkowski, "What Mass Are the Smallest Protohalos?," *Phys. Rev. Lett.* **97**, 031301 (2006). DOI: 10.1103/PhysRevLett.97.031301
85. J. Zavala, M. Vogelsberger, and M. G. Walker, "Constraining Self-Interacting Dark Matter with the Milky Way's Dwarf Spheroidals," *Mon. Not. R. Astron. Soc.* **405**, 593 (2010). DOI: 10.1111/j.1745-3933.2010.00843.x
86. M. Ackermann et al. (Fermi-LAT), "Search for Extended Sources in the Galactic Plane Using Six Years of Fermi-LAT Pass 8 Data above 10 GeV," *Astrophys. J.* **840**, 43 (2017). DOI: 10.3847/1538-4357/aa6cab
87. J. McDonald, "Thermally Generated Gauge Singlet Scalars as Self-Interacting Dark Matter," *Phys. Rev. D* **48**, 2462 (1993). DOI: 10.1103/PhysRevD.48.2462
88. Y. Nomura, M. Papucci, and D. Stolarski, "Phenomenology of Light Higgsinos," *Phys. Rev. D* **77**, 075006 (2008). DOI: 10.1103/PhysRevD.77.075006
89. S. R. Coleman and E. J. Weinberg, "Radiative Corrections as the Origin of Spontaneous Symmetry Breaking," *Phys. Rev. D* **7**, 1888 (1973). DOI: 10.1103/PhysRevD.7.1888
90. D. N. Spergel and P. J. Steinhardt, "Observational Evidence for Self-Interacting Cold Dark Matter," *Phys. Rev. Lett.* **84**, 3760 (2000). DOI: 10.1103/PhysRevLett.84.3760
91. S. Tulin, H.-B. Yu, and K. M. Zurek, "Beyond Collisionless Dark Matter: Particle Physics Dynamics for Dark Matter Halo Structure," *Phys. Rev. D* **87**, 115007 (2013). DOI: 10.1103/PhysRevD.87.115007
92. J. Zavala, M. Vogelsberger, and M. G. Walker, "Constraining Self-Interacting Dark Matter with the Milky Way's Dwarf Spheroidals," *Mon. Not. R. Astron. Soc.* **405**, 593 (2010). DOI: 10.1111/j.1745-3933.2010.00843.x
93. F.-Y. Cyr-Racine, R. de Putter, A. Raccanelli, and K. Sigurdson, "Constraints on Large-Scale Dark Acoustic Oscillations from Current CMB Data," *Phys. Rev. D* **89**, 063517 (2014). DOI: 10.1103/PhysRevD.89.063517
94. A. Robertson et al., "The Effect of Galaxy Formation on the Slope of the Dark Matter Halo Mass Function and the Power Spectrum," *Mon. Not. R. Astron. Soc.* **465**, 569 (2017). DOI: 10.1093/mnras/stw2670

95. K. Petraki and R. R. Volkas, "Review of Asymmetric Dark Matter," *Int. J. Mod. Phys. A* **28**, 1330028 (2013). DOI: 10.1142/S0217751X13300287
96. A. Sakharov, "Violation of *CP* Invariance, *C* Asymmetry, and Baryon Asymmetry of the Universe," *JETP Lett.* **5**, 24 (1967). https://www.osti.gov/biblio/4449128
97. C. Caprini et al., "Science with the Space-Based Interferometer eLISA. II: Gravitational Waves from Cosmological Phase Transitions," *J. Cosmol. Astropart. Phys.* **04**, 001 (2016). DOI: 10.1088/1475-7516/2016/04/001
98. P. Amaro-Seoane et al. (LISA), "Laser Interferometer Space Antenna," *arXiv:1702.00786* (2017). arXiv:1702.00786
99. B. Carr, F. Kuhnel, and M. Sandstad, "Primordial Black Holes as Dark Matter," *Phys. Rev. D* **94**, 083504 (2016). DOI: 10.1103/PhysRevD.94.083504
100. M. Ricotti, J. P. Ostriker, and K. J. Mack, "Effect of Primordial Black Holes on the Cosmic Microwave Background and Cosmological Parameter Estimates," *Astrophys. J.* **680**, 829 (2008). DOI: 10.1086/587831
101. J. L. Hewett and T. G. Rizzo, "Low-Energy Phenomenology of Superstring-Inspired E_6 Models," *Phys. Rep.* **183**, 193 (1989). DOI: 10.1016/0370-1573(89)90071-9
102. L. E. Ibáñez and A. M. Uranga, *String Theory and Particle Physics* (Cambridge University Press, Cambridge, 2012). DOI: 10.1017/CBO9781139018951
103. E. Hairer and G. Wanner, *Solving Ordinary Differential Equations II: Stiff Problems* (Springer, Berlin, 1996). DOI: 10.1007/978-3-642-05221-7
104. A. Gelman and D. B. Rubin, "Inference from Iterative Simulation Using Multiple Sequences," *Stat. Sci.* **7**, 457 (1992). DOI: 10.1214/ss/1177011136
105. S. P. Brooks and A. Gelman, "General Methods for Monitoring Convergence of Iterative Simulations," *J. Comput. Graph. Stat.* **7**, 434 (1998). DOI: 10.1080/10618600.1998.10474787
106. J. P. Delahaye et al., "Muon Collider: A Path to the Energy Frontier," *arXiv:1901.06150* (2019). arXiv:1901.06150
107. A. Abada et al. (FCC Collaboration), "FCC-ee: The Lepton Collider," *Eur. Phys. J. C* **79**, 474 (2019). DOI: 10.1140/epjc/s10052-019-6904-3
108. ATLAS Collaboration, "Search for Long-Lived Particles Decaying into Displaced Vertices in the ATLAS Inner Detector," *Phys. Lett. B* **793**, 499 (2019). DOI: 10.1016/j.physletb.2019.04.024
109. LHC Higgs Cross Section WG, "Handbook of LHC Higgs Cross Sections: 4. Deciphering the Nature of the Higgs Sector," *CERN Yellow Rep. Monogr.* **2**, 1 (2016). DOI: 10.23731/CYRM-2017-002
110. ATLAS Collaboration, "Search for Charginos and Neutralinos in Final States with Two Boosted Hadronically Decaying Bosons," *JHEP* **05**, 044 (2019). DOI: 10.1007/JHEP05(2019)044
111. R. D. Ball et al. (NNPDF), "Parton Distributions from High-Precision Collider Data," *Eur. Phys. J. C* **77**, 663 (2017). DOI: 10.1140/epjc/s10052-017-5199-5
112. D. Rainwater and T. Plehn, "Probing Color-Octet Couplings of the Higgs Boson at the LHC," *Phys. Rev. D* **90**, 115022 (2014). DOI: 10.1103/PhysRevD.90.115022
113. M. Anselmino et al., "The Theory and Phenomenology of Polarized Deep Inelastic Scattering," *Rev. Mod. Phys.* **65**, 1199 (1993). DOI: 10.1103/RevModPhys.65.1199
114. L. Maiani et al., "Diquark-Antidiquark States with Hidden or Open Charm and the Nature of $X(3872)$," *Phys. Rev. D* **89**, 114010 (2014). DOI: 10.1103/PhysRevD.89.114010
115. R. F. Lebed, R. E. Mitchell, and E. S. Swanson, "Heavy-Quark QCD Exotica," *Prog. Part. Nucl. Phys.* **93**, 143 (2017). DOI: 10.1016/j.ppnp.2016.11.003
116. CMS Collaboration, "Search for Electroweak Production of Charginos and Neutralinos in Multilepton Final States in pp Collisions at $\sqrt{s} = 13$ TeV," *JHEP* **03**, 141 (2017). DOI: 10.1007/JHEP03(2017)141
117. W. Altmannshofer et al. (Belle-II), "The Belle II Physics Book," *PTEP* **2019**, 123C01 (2019). DOI: 10.1093/ptep/ptz106
118. G. Altarelli, R. Barbieri, and F. Caravaglios, "Electroweak Precision Tests: A Concise Review," *Phys. Lett. B* **349**, 145 (1995). DOI: 10.1016/0370-2693(95)00179-O
119. T. Behnke et al., "The International Linear Collider Technical Design Report Volume 1: Executive Summary," *arXiv:1306.6327* (2013). arXiv:1306.6327
120. CEPC Study Group, "CEPC Conceptual Design Report: Volume 2 Physics & Detector," *arXiv:1809.00285* (2018). arXiv:1809.00285
121. M. Cirelli, N. Fornengo, and A. Strumia, "Minimal Dark Matter," *Nucl. Phys. B* **753**, 178 (2006). DOI: 10.1016/j.nuclphysb.2006.07.012
122. ATLAS Collaboration, "Search for Heavy Long-Lived Charged *R*-Hadrons with the ATLAS Detector in pp Collisions at $\sqrt{s} = 13$ TeV," *Phys. Rev. D* **98**, 032016 (2018). DOI: 10.1103/PhysRevD.98.032016

123. D. Barducci et al., "Monojet Searches for Momentum-Dependent Dark Matter Interactions," *Phys. Rev. D* **99**, 035043 (2019). DOI: 10.1103/PhysRevD.99.035043
124. U. Haisch, F. Kahlhoefer, and E. Re, "QCD Effects in Mono-Jet Searches for Dark Matter," *JHEP* **12**, 007 (2013). DOI: 10.1007/JHEP12(2013)007
125. ATLAS Collaboration, "Search for Long-Lived Particles Produced in pp Collisions at $\sqrt{s} = 13$ TeV that Decay into Displaced Hadronic Jets in the ATLAS Muon Spectrometer," *Phys. Rev. D* **99**, 052005 (2019). DOI: 10.1103/PhysRevD.99.052005
126. CMS Collaboration, "Search for New Physics in Dijet Angular Distributions Using Proton-Proton Collisions at $\sqrt{s} = 13$ TeV and Constraints on Dark Matter and Other Models," *JHEP* **10**, 073 (2017). DOI: 10.1007/JHEP10(2017)073
127. ATLAS Collaboration, "Search for Dark Matter Produced in Association with a Higgs Boson Decaying to Two Bottom Quarks in pp Collisions at $\sqrt{s} = 8$ TeV with the ATLAS Detector," *Eur. Phys. J. C* **78**, 18 (2018). DOI: 10.1140/epjc/s10052-017-5491-4
128. N. Brambilla et al., "QWG: Heavy Quarkonium Physics," *Eur. Phys. J. C* **74**, 2981 (2014). DOI: 10.1140/epjc/s10052-014-2981-5
129. A. Esposito et al., "Multiquark Resonances," *Phys. Rep.* **668**, 1 (2016). DOI: 10.1016/j.physrep.2016.11.002
130. B. Field, S. Dawson, and J. Smith, "Scalar Quark Contributions to Higgs Boson Plus Two Jet Production," *Phys. Rev. D* **69**, 074013 (2004). DOI: 10.1103/PhysRevD.69.074013
131. P. Artoisenet and E. Braaten, "Production of J/ψ at High Transverse Momentum at the Tevatron," *Phys. Rev. D* **81**, 114018 (2010). DOI: 10.1103/PhysRevD.81.114018
132. ATLAS Collaboration, "Search for Non-Resonant Higgs Boson Pair Production in the $bb\ell\nu\ell\nu$ Final State with the ATLAS Detector," *JHEP* **10**, 182 (2019). DOI: 10.1007/JHEP10(2019)182
133. CMS Collaboration, "Search for Higgs Boson Pair Production in the $b\bar{b}\tau^+\tau^-$ Final State," *JHEP* **06**, 128 (2018). DOI: 10.1007/JHEP06(2018)128
134. CMS Collaboration, "Search for Higgs Boson Pair Production in the Four b Quark Final State," *Phys. Lett. B* **802**, 135262 (2020). DOI: 10.1016/j.physletb.2020.135262
135. ATLAS Collaboration, "Search for Pair Production of Higgs Bosons in the $b\bar{b}b\bar{b}$ Final State Using Proton-Proton Collisions at $\sqrt{s} = 13$ TeV with the ATLAS Detector," *Phys. Rev. D* **96**, 052004 (2017). DOI: 10.1103/PhysRevD.96.052004
136. CMS Collaboration, "Search for Resonant and Nonresonant Higgs Boson Pair Production in the $b\bar{b}\ell\nu\ell\nu$ Final State in pp Collisions at $\sqrt{s} = 13$ TeV," *JHEP* **07**, 014 (2017). DOI: 10.1007/JHEP07(2017)014
137. P. Fileviez Pérez and M. B. Wise, "Baryon and Lepton Number as Local Gauge Symmetries," *Phys. Rev. D* **80**, 053006 (2009). DOI: 10.1103/PhysRevD.80.053006
138. M. Baak et al. (Gfitter Group), "The Global Electroweak Fit at NNLO and Prospects for the LHC and ILC," *Eur. Phys. J. C* **74**, 3046 (2014). DOI: 10.1140/epjc/s10052-014-3046-5
139. PDG Collaboration, "Review of Particle Physics," *Prog. Theor. Exp. Phys.* **2022**, 083C01 (2022). DOI: 10.1093/ptep/ptac097
140. PDG Collaboration, "Review of Particle Physics" [electroweak fits; same volume as Ref. [139]], *Prog. Theor. Exp. Phys.* **2022**, 083C01 (2022). DOI: 10.1093/ptep/ptac097
141. K. Jedamzik, "Did Something Decay, Evaporate, or Annihilate during Big Bang Nucleosynthesis?," *Phys. Rev. D* **74**, 103509 (2006). DOI: 10.1103/PhysRevD.74.103509
142. D. J. Fixsen et al., "The Cosmic Microwave Background Spectrum from the Full COBE FIRAS Data Set," *Astrophys. J.* **473**, 576 (1996). DOI: 10.1086/178173
143. J. A. Dror, E. Kuflik, and W. H. Ng, "Codecaying Dark Matter," *Phys. Rev. Lett.* **117**, 211801 (2016). DOI: 10.1103/PhysRevLett.117.211801
144. M. Drees, F. Hajkarim, and E. R. Schmitz, "The Effects of QCD Equation of State on the Relic Density of WIMP Dark Matter," *JCAP* **06**, 025 (2015). DOI: 10.1088/1475-7516/2015/06/025
145. P. F. de Salas and S. Pastor, "Relic Neutrino Decoupling with Flavour Oscillations Revisited," *JCAP* **07**, 051 (2016). DOI: 10.1088/1475-7516/2016/07/051
146. A. Fradette, M. Pospelov, J. Pradler, and A. Ritz, "Cosmological Beam Dump: Constraints on Dark Scalars Mixed with the Higgs Boson," *Phys. Rev. D* **99**, 075004 (2019). DOI: 10.1103/PhysRevD.99.075004
147. A. Fattahi et al., "The APOSTLE Simulations: Solutions to the Local Group's Cosmic Puzzles," *Mon. Not. R. Astron. Soc.* **457**, 844 (2016). DOI: 10.1093/mnras/stv2970
148. E. Tollet et al., "NIHAO IV: Core Creation and Destruction in Dark Matter Density Profiles across Cosmic Time," *Mon. Not. R. Astron. Soc.* **456**, 3542 (2016). DOI: 10.1093/mnras/stv2856

149. B. W. Keller et al., "Kinematics as an Astrophysical Probe of Dark Matter," *Mon. Not. R. Astron. Soc.* **482**, 2244 (2019). DOI: 10.1093/mnras/sty2859
150. S. Garrison-Kimmel et al., "Not as Big as We Thought: The Role of Baryons in Shaping the Radial Acceleration of Milky Way Satellites," *Mon. Not. R. Astron. Soc.* **471**, 1709 (2017). DOI: 10.1093/mnras/stx1710
151. D. Harvey et al., "The Nongravitational Interactions of Dark Matter in Colliding Galaxy Clusters," *Science* **347**, 1462 (2015). DOI: 10.1126/science.1261381
152. R. Massey et al., "The Behaviour of Dark Matter Associated with Four Bright Cluster Galaxies in the 10 kpc Core of Abell 3827," *Mon. Not. R. Astron. Soc.* **449**, 3393 (2015). DOI: 10.1093/mnras/stv467
153. F. Kahlhoefer et al., "Colliding Clusters and Dark Matter Self-Interactions," *Mon. Not. R. Astron. Soc.* **452**, L54 (2015). DOI: 10.1093/mnrasl/slv088
154. O. D. Elbert et al., "A Quantitative Comparison of Simulated and Observed Galaxy Clusters from the Local Volume," *Astrophys. J.* **853**, 109 (2018). DOI: 10.3847/1538-4357/aa9710
155. G. Cowan, K. Cranmer, E. Gross, and O. Vitells, "Asymptotic Formulae for Likelihood-Based Tests of New Physics," *Eur. Phys. J. C* **71**, 1554 (2011). DOI: 10.1140/epjc/s10052-011-1554-0
156. A. Gelman et al., *Bayesian Data Analysis*, 3rd ed. (CRC Press, Boca Raton, 2013). DOI: 10.1201/b16018
157. M. Vogelsberger, J. Zavala, and A. Loeb, "Subhaloes in Self-Interacting Galactic Dark Matter Haloes," *Mon. Not. R. Astron. Soc.* **423**, 3740 (2012). DOI: 10.1111/j.1365-2966.2012.21182.x
158. K. A. Oman et al., "The Unexpected Diversity of Dwarf Galaxy Rotation Curves," *Mon. Not. R. Astron. Soc.* **452**, 3650 (2015). DOI: 10.1093/mnras/stv1504
159. J. F. Navarro et al., "The Origin of the Mass Discrepancy–Acceleration Relation in ΛCDM," *Mon. Not. R. Astron. Soc.* **471**, 1841 (2017). DOI: 10.1093/mnras/stx1705
160. J. I. Read, M. G. Walker, and P. Steger, "Dark Matter Heats Up in Dwarf Galaxies," *Mon. Not. R. Astron. Soc.* **481**, 860 (2018). DOI: 10.1093/mnras/sty2286
161. S. Tremaine and J. E. Gunn, "Dynamical Role of Light Neutral Leptons in Cosmology," *Phys. Rev. Lett.* **42**, 407 (1979). DOI: 10.1103/PhysRevLett.42.407
162. T. Bringmann, F. Kahlhoefer, K. Schmidt-Hoberg, and P. Walia, "Does NANOGrav Observe a Dark Matter Subhalo Next to Earth?," *Phys. Rev. D* **98**, 023543 (2018). DOI: 10.1103/PhysRevD.98.023543
163. M. Kaplinghat, S. Tulin, and H.-B. Yu, "Direct Detection Portals for Self-Interacting Dark Matter," *Phys. Rev. D* **89**, 035009 (2014). DOI: 10.1103/PhysRevD.89.035009
164. J. Zavala, M. R. Lovell, M. Vogelsberger, and J. Burger, "ETHOS An Effective Theory of Structure Formation: Detecting Dark Matter Interactions through the Lyman-α Forest," *Phys. Rev. D* **100**, 063007 (2019). DOI: 10.1103/PhysRevD.100.063007
165. J. Lesgourgues, G. Mangano, G. Miele, and S. Pastor, *Neutrino Cosmology* (Cambridge University Press, Cambridge, 2013). DOI: 10.1017/CBO9781139012874
166. M. Betoule et al. (SDSS), "Improved Cosmological Constraints from a Joint Analysis of the SDSS-II and SNLS Supernova Samples," *Astron. Astrophys.* **568**, A22 (2014). DOI: 10.1051/0004-6361/201423413
167. S. Nadathur et al., "Beyond BAO: Improving Cosmological Constraints from BOSS Data with Measurement of the Void-Galaxy Cross-Correlation," *Phys. Rev. D* **100**, 023504 (2019). DOI: 10.1103/PhysRevD.100.023504
168. T. M. C. Abbott et al. (DES), "Dark Energy Survey Year 1 Results: Cosmological Constraints from Galaxy Clustering and Weak Lensing," *Phys. Rev. D* **98**, 043526 (2018). DOI: 10.1103/PhysRevD.98.043526
169. D. J. Marsh, "Axion Cosmology," *Phys. Rep.* **643**, 1 (2016). DOI: 10.1016/j.physrep.2016.06.005
170. A. Borde and F. J. Sanchez-Salcedo, "Dark Matter Distribution in the Milky Way: Constraints from the Observed Kinematics of the Local Halo," *JCAP* **02**, 002 (2006). DOI: 10.1088/1475-7516/2006/02/002
171. L. E. Strigari et al., "A Common Mass Scale for Satellite Galaxies of the Milky Way," *Astrophys. J.* **678**, 614 (2008). DOI: 10.1086/529488
172. R. A. C. Croft et al., "Toward a Precise Measurement of Matter Clustering: Lyα Forest Data at Redshifts 2–4," *Astrophys. J.* **581**, 20 (2002). DOI: 10.1086/344099
173. A. W. McConnachie, "The Observed Properties of Dwarf Galaxies in and around the Local Group," *Astron. J.* **144**, 4 (2012). DOI: 10.1088/0004-6256/144/1/4
174. M. Milgrom, "A Modification of the Newtonian Dynamics as a Possible Alternative to the Hidden Mass Hypothesis," *Astrophys. J.* **270**, 365 (1983). DOI: 10.1086/161130
175. F. Lelli, S. S. McGaugh, and J. M. Schombert, "SPARC: Mass Models for 175 Disk Galaxies with Spitzer Photometry and Accurate Rotation Curves," *Astron. J.* **152**, 157 (2016). DOI: 10.3847/0004-6256/152/6/157
176. B. Famaey and S. McGaugh, "Modified Newtonian Dynamics (MOND): Observational Phenomenology and Relativistic Extensions," *Living Rev. Relativ.* **15**, 10 (2012). DOI: 10.12942/lrr-2012-10

177. J. D. Bekenstein, "Relativistic Gravitation Theory for the Modified Newtonian Dynamics Paradigm," *Phys. Rev. D* **70**, 083509 (2004). DOI: 10.1103/PhysRevD.70.083509
178. G. Belanger, A. Pukhov, and G. Servant, "Dirac Neutrino Dark Matter," *JCAP* **01**, 009 (2008). DOI: 10.1088/1475-7516/2008/01/009
179. D. Eckert, S. Ettori,, "Constraints on dark matter self-interaction from the internal density profiles of X-COP galaxy clusters," *Astrophys. J.* **A&A 666, A41 (2022)**. DOI: 10.1051/0004-6361/202243205
180. P. A. Oesch et al., "A Remarkably Luminous Galaxy at $z = 11.1$ Measured with Hubble Space Telescope Grism Spectroscopy," *Astrophys. J.* **819**, 129 (2016). DOI: 10.3847/0004-637X/819/2/129
181. P. Madau and M. Dickinson, "Cosmic Star-Formation History," *Annu. Rev. Astron. Astrophys.* **52**, 415 (2014). DOI: 10.1146/annurev-astro-081811-125615
182. Y. Sofue and V. Rubin, "Rotation Curves of Spiral Galaxies," *Annu. Rev. Astron. Astrophys.* **39**, 137 (2001). DOI: 10.1146/annurev.astro.39.1.137
183. G. Jungman, M. Kamionkowski, and K. Griest, "Supersymmetric Dark Matter" [see also Ref. [34]], *Phys. Rep.* **267**, 195 (1996). DOI: 10.1016/0370-1573(95)00058-5
184. K. R. Dienes, "String Theory and the Path to Unification: A Review of Recent Developments," *Phys. Rep.* **287**, 447 (1997). DOI: 10.1016/S0370-1573(97)00009-4
185. P. Bari, A. Ricciardone, N. Bartolo, D. Bertacca, and S. Matarrese, "Signatures of Primordial Gravitational Waves on the Large-Scale Structure of the Universe," *Phys. Rev. Lett.* **129**, 091301 (2022). DOI: 10.1103/PhysRevLett.129.091301
186. W. Hu and M. Tegmark, "Measuring Cosmological Parameters with Galaxy Surveys," *Astrophys. J.* **514**, L65 (1999). DOI: 10.1086/311947
187. J. Goodman et al., "Constraints on Dark Matter from Colliders," *Phys. Rev. D* **82**, 116010 (2010). DOI: 10.1103/PhysRevD.82.116010
188. G. Arcadi et al., "The Waning of the WIMP? A Review of Models, Searches, and Constraints" [see also Ref. [74]], *Eur. Phys. J. C* **78**, 203 (2018). DOI: 10.1140/epjc/s10052-018-5662-y
189. K. Griest, "Galactic Searchers for Dark Matter," *Phys. Rev. D* **38**, 2357 (1988). DOI: 10.1103/PhysRevD.38.2357
190. D. N. Spergel and P. J. Steinhardt, "Observational Evidence for Self-Interacting Cold Dark Matter" [see also Ref. [90]], *Phys. Rev. Lett.* **84**, 3760 (2000). DOI: 10.1103/PhysRevLett.84.3760
191. S. Tulin, H.-B. Yu, and K. M. Zurek, "Resonant Dark Forces and Small-Scale Structure," *Phys. Rev. Lett.* **110**, 111301 (2013). DOI: 10.1103/PhysRevLett.110.111301
192. J. L. Feng, M. Kaplinghat, H. Tu, and H.-B. Yu, "Hidden Charged Dark Matter," *JCAP* **07**, 004 (2009). DOI: 10.1088/1475-7516/2009/07/004
193. A. Robertson et al., "Cosmic Particle Colliders: Simulations of Self-Interacting Dark Matter with Anisotropic Scattering," *Mon. Not. R. Astron. Soc.* **467**, 4719 (2017). DOI: 10.1093/mnras/stx463
194. M. Boylan-Kolchin, V. Springel, S. D. M. White, A. Jenkins, and G. Lemson, "Resolving Cosmic Structure Formation with the Millennium-II Simulation," *Mon. Not. R. Astron. Soc.* **398**, 1150 (2009). DOI: 10.1111/j.1365-2966.2009.15191.x
195. A. Brooks and A. Zolotov, "Why Baryons Matter: The Role of Galactic Feedback on the Abundance and Kinematics of Satellites," *Astrophys. J.* **786**, 87 (2014). DOI: 10.1088/0004-637X/786/2/87
196. K. Popper, *The Logic of Scientific Discovery* (doi.org/10.4324/9780203994627
197. E. C. G. Stückelberg, "Die Wechselwirkungskräfte in der Elektrodynamik und in der Feldtheorie der Kräfte," *Helv. Phys. Acta* **273**, 225 (2009). https://ui.adsabs.harvard.edu/abs/2009esuf.book..273
198. B. Kors and P. Nath, "A Stückelberg Extension of the Standard Model," *Phys. Lett. B* **586**, 366 (2004). DOI: 10.1016/j.physletb.2004.02.051
199. G. 't Hooft, "Computation of the Quantum Effects Due to a Four-Dimensional Pseudoparticle," *Phys. Rev. Lett.* **37**, 8 (1976). DOI: 10.1103/PhysRevLett.37.8
200. T. H. R. Skyrme, "A Unified Field Theory of Mesons and Baryons," *Nucl. Phys.* **31**, 556 (1962). DOI: 10.1016/0029-5582(62)90775-7
201. P. de Forcrand and O. Jahn, "Comparison of SO(3) and SU(2) lattice gauge theory," *Nucl. Phys. B* **651**, 125 (2003). DOI: 10.1016/S0550-3213(02)01123-9
202. W. Hurewicz and H. Wallman, *Dimension Theory* (Princeton University Press, Princeton, NJ, 1941). DOI: 10.1515/9781400875665